tutor/s

Dr. Roger Bringué
Departament of Chemical Engineering and Analytical Chemistry

Dr. Carles Fité
Departament of Chemical Engineering and Analytical Chemistry

Grau en Enginyeria Química

Treball Final de Grau

Kinetic study of 5-nonanol intramolecular dehydration to nonenes over Amberlyst 45: effect of water.

Florencia María, Moreya

June 2022

UNIVERSITAT DE BARCELONA

With two adjustable parameters, I can fit an elephant, with three a running elephant.

John von Neumann

En primer lugar, quiero agradecer a mi familia por el apoyo incondicional a lo largo de toda esta etapa. A mis amigos, los nuevos que he hecho aquí y los que me siguen apoyando a distancia. Por último, agradecer a los profesores que me han guiado durante todo el grado, en especial al Dr. Roger Bringué y Dr. Carles Fité con quienes he realizado este trabajo.

.

.

CONTENTS

SUMMARY i
RESUM ii
THE SUSTAINABLE DEVELOPMENT GOAL iii
1. INTRODUCTION 1
1.1. FROM LIGNOCELLULOSIC TO BIOFUEL 2
1.2. 5-NONANOL DEHYDRATION INTO NONENE 4
1.3. ION-EXCHANGE RESINS 4
1.4. KINETIC MODELS 5
1.5. STATE-OF-THE-ART ALCOHOL DEHYDRATION KINETIC MODELS 8
1.6. INFLUENCE OF WATER 8
2. OBJECTIVES 9
3. ANALYSIS OF REACTION RATES ON ACTIVITIES 11
4. DEVELOPMENT OF MATHEMATICAL MODELS 17
5. RESULTS AND DISCUSSION 23
6. CONCLUSIONS 45
7. RECOMMENDATIONS 46
REFERENCES AND NOTES 47
ACRONYMS 49

APPENDICES 51

APPENDIX 1: TABLES WITH ALL MODELS ANALYZED. 53

APPENDIX 2: MODELS MODIFIED BY THE ADDITION OF WATER INHIBITION FIGURES 57

SUMMARY

Due to climate change, as well as the strong dependence on fossil fuels in our society, in recent years, pathways to obtain biofuels have been studied. One of the most developed pathways is to obtain biofuels from lignocellulose. A series of reactions are involved in this pathway, one of these is 5-nonanol dehydration to obtain nonenes. Nonenes are usually used to improve gasoline blending. The present work focuses on developing a kinetic model that explains satisfactorily 5-nonanol dehydration over certain experimental conditions but also, that had a thermodynamical basis to be extrapolated to other operational conditions.

To fulfill the objective, a mechanism based on Langmuir-Hinshelwood-Hougen-Watson formulism was proposed to find a general expression for reaction rate. The surface reaction was assumed to be a rate-controlling step. Then, 75 equations have been obtained by proposing different variations of the general expression of the reaction rate. Following, experimental data were fitted using those expressions to find parameters models. Then, parameter and values rate prediction by models has been analyzed under a selection criterion. An inhibition factor was applied to the set of best models previously founded. Finally, 10 more equations have been analyzed. Activation energy estimated from models was compared to activation energy found in the literature for similar systems.

Keywords: Kinetic modeling, Amberlyst™ 45, inhibiting effect, water, 5-nonanol, dehydration, nonenes.

RESUMEN

Debido al cambio climático y a la fuerte dependencia de los combustibles fósiles en nuestra sociedad, se han estudiado formas de obtener biocombustibles en los últimos años. Una de las vías más desarrolladas es la obtención de biocombustibles a partir de lignocelulosa. En esta vía intervienen una serie de reacciones, una de las cuales es la deshidratación del 5-nonanol para obtener nonenos. Los nonenos se utilizan generalmente para mejorar la mezcla de gasolina. El presente trabajo se enfoca en desarrollar un modelo cinético que explique satisfactoriamente la deshidratación del 5-nonanol bajo ciertas condiciones experimentales pero que también tenga una base termodinámica para ser extrapolable a otras condiciones de operación.

Para cumplir con el objetivo se propuso un mecanismo basado en el empirismo de Langmuir-Hinshelwood-Hougen-Watson para encontrar una expresión general para la velocidad de reacción. Se supuso que la reacción superficial era la etapa controlante de velocidad. Así, se han obtenido 75 ecuaciones proponiendo distintas variaciones de la expresión general de la velocidad de reacción. Luego, para encontrar los parámetros de los modelos se ajustaron los datos experimentales usando esas expresiones. A continuación, los parámetros y valores velocidad de reacción predichos por los modelos han sido analizados bajo un criterio de selección. Por último, se aplicó un factor de inhibición al conjunto de mejores modelos encontrados previamente dando lugar a 10 ecuaciones que también han sido analizadas. La energía de activación estimada a partir de los modelos se comparó con la energía de activación encontrada en la literatura para sistemas similares.

Palabras clave: Modelado cinético, AmberlystTM 45, efecto inhibidor, agua, 5-nonanol, deshidratación, nonenos.

THE SUSTAINABLE DEVELOPMENT GOALS

The present work focuses on developing a kinetic model of 5-nonanol dehydration. This reaction is one step of a complex pathway to obtain biofuel from biomass. The development of thermodynamically consistent models allows its application in different operational conditions from which it was deducted. These models are needed for reactor designs in the industry. Then, the development of this model is necessary for the industrial production of biofuel from biomass. This project is related to 3P: planet, people, and prosperity. The production of biofuel reduced the gas concentration of greenhouse gases (GHGs) and help reduce global warming. Furthermore, global warming and climate change have created a variety of problems for endangered species and caused a rise in pests and diseases that may have an impact on human health. Lastly, the use of biofuel is a more sustainable energy source.

1. INTRODUCTION

The overuse of fossil fuels as energy resources is a main cause of global warming, because it increases the concentration of greenhouse gases (GHGs), such as CO_2, CH_4, N_2O, in the atmosphere. Among them, the concentration of CO_2 is the determining factor.[1]

Some of the adverse effects of climate change are the melting of ice and glaciers; increases in ocean temperatures and ocean acidity; weather imbalance, uncontrolled floods, drought seasons, and heat waves promoting more aggressive hurricanes. Furthermore, it has created a variety of problems for endangered species and causes a rise in pests and diseases that may have an impact on human health. Hence the importance of developing renewable fuels and biofuels obtained from biomass. [2]

Green energy production can be achieved from lignocellulose waste without affecting food supplies. As the most abundant renewable resource is economically viable. Its world production reaches 120×10^9 tons per year. However, most of it is burned in open field or disposed of as wastes, which decreases the quality of the environment and affects human health [3]. There are different types of biofuels depending on the biomass origin shown in Fig.1. Second-generation biofuels are obtained from green non-edible sources and the main source of biomass is lignocellulosic.

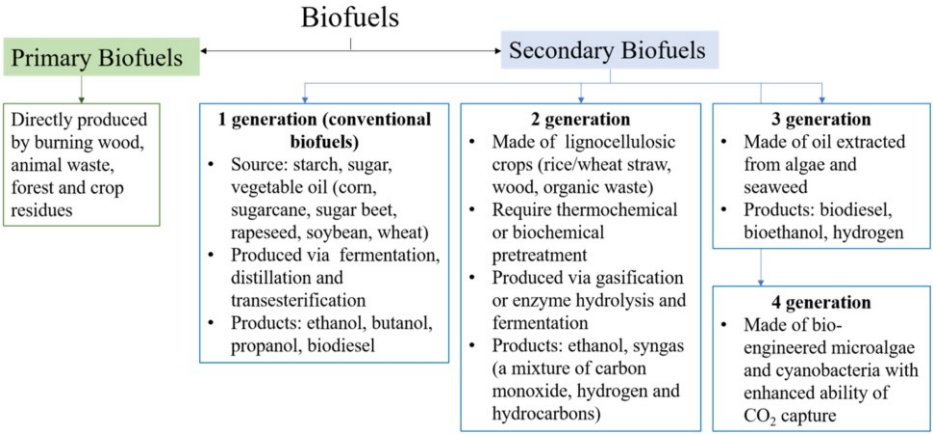

Figure 1. The summary scheme of biofuel generations (extracted from ref 4)

1.1. **FROM LIGNOCELLULOSIC TO BIOFUEL**

Lignocellulosic biomass is naturally difficult to biodegrade. Its composition includes lignin, cellulose and hemicellulose. These polymers can be hydrolyzed to C5-C6 sugars, which are the starting materials for great variety of reactions. During the last years, great effort is been dedicated to obtain valuable products from lignocellulosic biomass. Among these products, we find levulinic acid. Levulinic acid (4-oxopentanoic acid) is one of the most important compounds in the wide list of molecules derived from biomass due to its reactive nature, in addition to the fact that it can be produced from lignocelluloses wastes at low cost. The reaction scheme is shown in Fig 2.

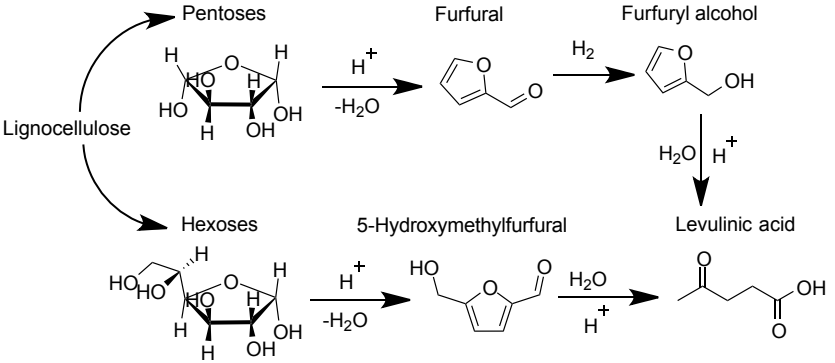

Figure 2 Production of levulinic acid from lignocellulose [3][9].

One important derivative from levulinic acid is the γ-valero lactone (GLV). There are two

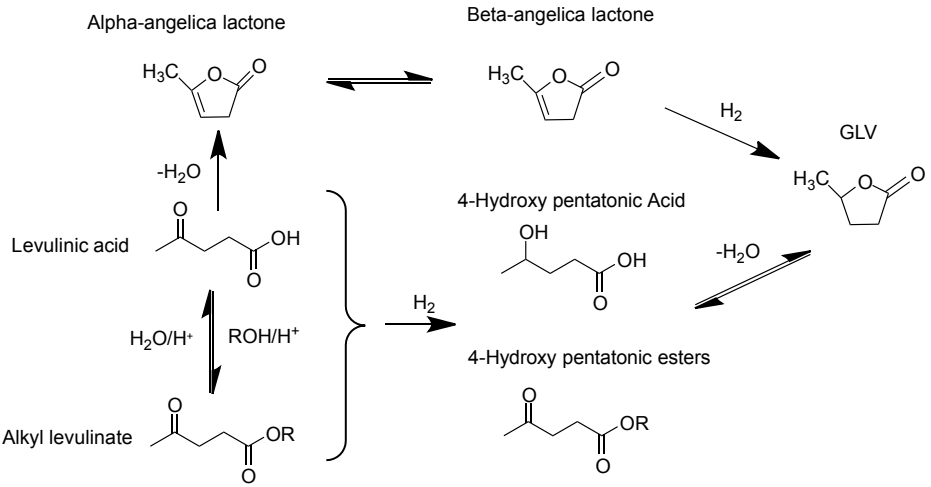

Figure 3. Routes for the production of gamma-valerolactone (GVL) [5][9]

routes to produce GVL from acid levulinic. The first one consists of the hydrogenation of levulinic acid (or its ester) to gamma-hydroxyvaleric acid (or ester). The subsequent intramolecular esterification produces GVL. The second route is the acid catalyzed dehydration of levulinic acid to angelica lactone followed by hydrogenation. Figure 3 illustrates both routes.

Figure 4 shows two routes to obtain hydrocarbon fuels from GLV. In route 2 pentanoic acid is produced through ring-opening/hydrogenation of GVL on a bifunctional (acid metal) catalyst. Following, ketonization of two molecules of pentanoic acid is carried out to obtain 5-nonanone with CO2 and water. Subsequently, 5-nonanone can be hydrogenated to 5-nonanol. Then, the alcohol is dehydrated and isomerized over an acid catalyst such as Amberlyst to produce nonene. Nonene is oligomerized to C18 alkenes. Finally, alkenes are hydrogenated to the corresponding alkanes to be used as a component in diesel. This work is focused on one particular step of this process, the 5-nonanol intramolecular dehydration to nonenes.

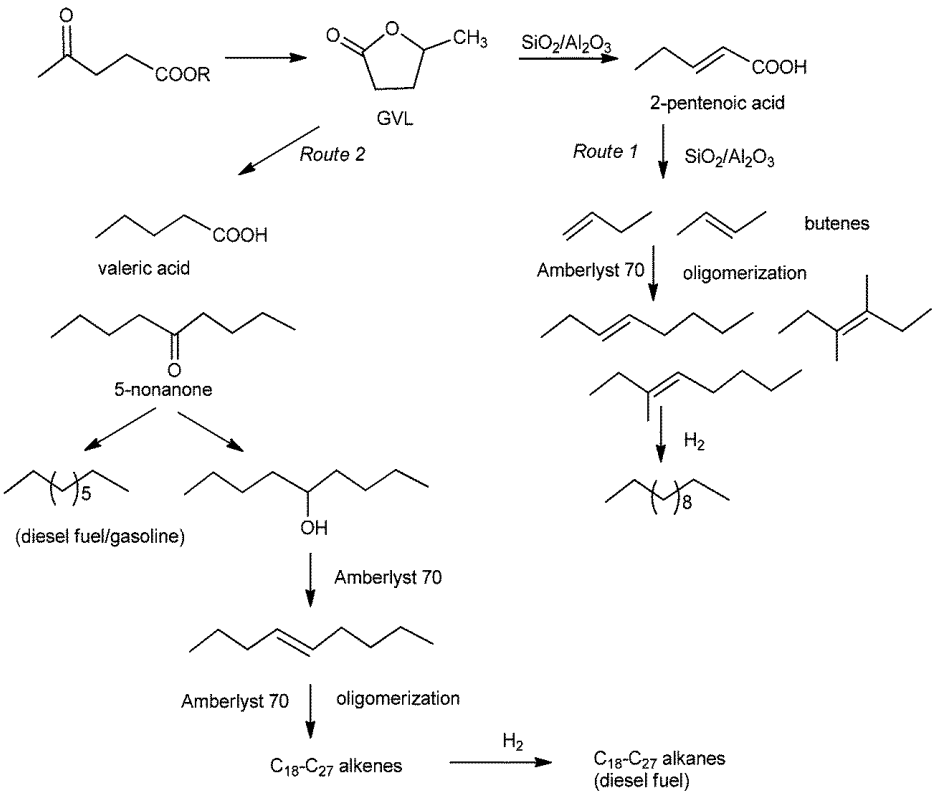

Figure 4. Routes for the transformation of GLV into liquid alkanes. (extracted from ref 5)

1.2. **5-NONANOL DEHYDRATION INTO NONENE**

The general reaction mechanism is illustrated in Figure 5. The reaction is carried out by a heterogeneous catalyst. In this case, it is an ion exchange resin composed of polystyrene-divinylbenzene (PS-DVB). The active centers of the catalyst are the sulfonic acid groups (-SO3H) that are anchored to the resin.

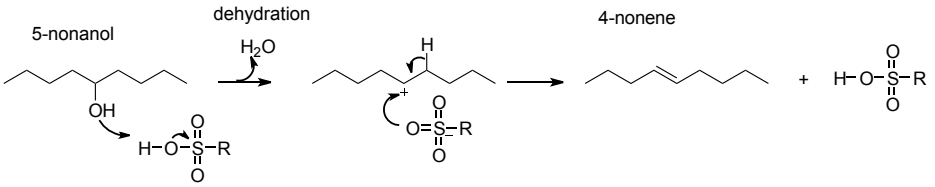

Figure 5 Dehydration of 5-nonanol with acidic ion-exchange resins.

1.3. **ION-EXCHANGE RESINS**

Polymeric matrix consists of hydrocarbon chains bonded together to form a three-dimensional hydrophobic crosslinked structure. The active centers are uniformly distributed in the matrix and are hydrophilic. Ion exchange resins are insoluble in solvents incapable of breaking hydrocarbon chains. Most ion exchange resins are manufactured from spherical polymeric beads synthesized by the procedure of suspension copolymerization, using styrene (ST) as polymerizing monomer and divinylbenzene (DVB) as cross-linking agent. The resins are sold in spherical form. Based on their structure P(S-DVB) resins can be classified into two main groups:

Gel-type resins:

These types of resins are hard glassy transparent beads. That is achieved by suspension polymerization with styrene and DVB. The percentage of DVB is usually between 0.5 to 20%.

The polymer chains are in molecular contact with each other, therefore, the resins have a very low surface area in the dry state, and the diffusion of even small molecules through this polymeric glass is very slow.

These materials will swell in a solvent with a solubility parameter similar to the polymer. The percentage swelling is typically inversely related to the DVB content or nominal crosslink ratio. Swelling creates space or 'solvent porosity' within the resin and allows access by small

molecules to the polymer network. The polymer network on the geometric exterior of resin beads becomes swollen first, forming an expanded pellicular layer and leaving a central unswollen glassy core. This process has been quantified using the so-called 'shrinking core' model. The reverse process of shrinkage can take place in certain solvents and results in material fatigue leading to breakage.

Macroreticular resins:

This type of resin is achieved when a suspension polymerization of a styrene–DVB mixture is carried out with the comonomer mixture also containing an appropriate organic solvent (diluent or porogen) at an accurate concentration. A porogen is a compound in which the monomer (styrene) is soluble but the polymer, as it is formed, is not. This introduces the mesopores and macropores during the copolymerization process.

The polymer matrix is rather heterogeneous or non-uniform. Some areas consist of impenetrable crosslinked and entangled polymer chains, other areas are devoid of polymer. That is why can be regarded as a combination of mass gel-type particles between a complex pore structure or labyrinth of channels.

In absence of swelling macroreticular resins contain pores partially stable. However, in the swollen state, macroreticular resins show three types of pores: non-swelling micropores, new mesoporous, and macroporous coming from permanent porosity. Therefore, the catalytic activity of macroreticular resins is effective in both swelling and non-swelling medium.

As an advantage, these resins have much higher surface areas in the dry state than gel-type resins.

Amberlyest 45 has been used to obtain the experimental data used in this work. It is a macroporous sulfonic acid polymer catalyst particularly well-suited for processes such as esterification, olefin hydration, and aromatic alkylation at temperatures of up to 170 ℃. It presents porosity independent on swelling. [6-10]

1.4. **KINETIC MODELS**

Proper knowledge of the kinetic model is needed for reactor design.

Levenspiel recommends that the simplest approach using first or nth-order rate expressions is good enough for engineering purposes. However, many researchers found that these

expressions do not come close to describing the experimental data and that adsorption/desorption effects should be included in the rate expressions.

Researchers in the resin catalysis field use either a pseudo homogeneous or a pseudo-heterogeneous approach to describe liquid phase surface reactions.

The pseudo-homogeneous model is based on the theory suggested by Helfferich in which the ions (mainly H+) are mobile and solvated and therefore a homogeneous solution can be assumed. The only difference in reaction mechanism in homogeneous catalysis by a dissolved electrolyte and heterogeneous catalysis is the internal and external diffusion processes.

However, many researchers follow a pseudo-heterogeneous approach to model the reaction kinetics. They use either a Langmuir–Hinshelwood or Eley–Rideal type expression to describe the reaction rate. These models account for adsorption of reactants and products onto the undissociated SO_3H+ groups on the resin surface. This occurs when the reaction mixture is not sufficiently polar for the SO_3H+ to be solvated, as a consequence, SO_3H+ is attached to the resin surface.

The kinetic model obtained when the true reaction mechanism is known can be used with guarantees in other conditions than those used for its determination. However, the fluids involved in industrial processes usually contain numerous substances that can participate in the reaction, so it is attempted to obtain models with a certain mechanistic basis.

Based on experience, it is known that the kinetic model of the reaction has a greater mechanistic basis when more is known about the microscopic and molecular character of the reactant system, nevertheless, the models obtained are more complex.

Generally, there are different classes of solid-catalyzed reaction models, those based on a reaction isotherm, those based on power law, and those that are a combination of these two.

The physical model to represent a catalytic reaction consists of 7 stages:

1. External mass transfer: diffusion of reactants from bulk liquid-phase to the external resin surface.
2. Internal mass transfer: diffusion of reactants through the catalyst (internal mass transfer).
3. Adsorption of reactants on resin active sites.

4. Surface reaction: chemical reaction between adsorbed species or between adsorbed species with fluid phase ones.
5. Desorption of reaction products.
6. Internal mass transfer: Diffusion of products through the catalyst.
7. External mass transfer: Diffusion of products from external resin surface to bulk liquid phase.

Steps 3, 4, and 5 are chemical, while steps 1, 2, 6, and 7 are physical steps of mass transfer. To obtain the kinetic model, it must be taken into account that steps 1, 3, 4, 5 and 7 are in series, while steps 2 and 6 run in series parallel with the previous ones. This is because some molecules may be diffusing into the pores while others have already reached the surface. The rate equations from the elementary steps are suitably combined to obtain the kinetic equation of the process. Simpler models can be obtained by considering that one of the steps is the controlling one, that is, the slowest step. To evaluate the resistance to mass transfer, the flow conditions (agitation) and the particle size of the catalyst are varied. If the physical steps are very fast, there is no resistance to mass transfer from the bulk liquid to the resin surface and from the resin surface to the active sites. Under these conditions, it can be assumed that the concentration around the catalyst sites is the same as that of the bulk liquid phase and the mass transfer steps do not affect the reaction rate of the catalytic reaction. Consequently, the overall reaction rate is that of the surface reaction and can be calculated from the reaction mechanism assuming that the concentration at the catalyst site is the same as that of the liquid surrounding the catalyst sites.

One of the most widely used isotherms is the Langmuir isotherm, from which the Langmuir-Hinshelwood models stem. These models are developed based on species concentration near active sites instead of occupied sites fraction. The kinetic expressions obtained by these models are based on the following hypotheses:

- The catalyst surface has a fixed number of active centers.
- All active sites are identical.
- The reactivity of the active sites does not depend on the nature or amount of other materials present on the surface during the reaction. It just depends on the temperature.

Variations can be proposed from a kinetic model, so it is mandatory to verify all of them to reach those that best fit the experimental reaction rate data and thus, be able to obtain the values of thermodynamic parameters. In general, all models have the same general structure (equation 1), where the number of actives sites involved in the reaction rate controlling stage is expressed by "n" [10,11,12].

$$reaction\ rate = \frac{[kinetic\ term][driving\ force]}{[adsortion\ term]^n} \qquad [1]$$

1.5. **STATE-OF-THE-ART ALCOHOL DEHYDRATION KINETIC MODELS**

The oligomerization of C9 alkenes produced from biomass-derived GVL has been studied. In this process, it has been found that alcohols in the feed, such as 5-nonanol, undergo dehydration under reaction conditions to produce water, which has a strongly inhibiting effect on the rate of alkene oligomerization. The effect of nonanol impurities into nonene was studied over Amberlyst-70 but no kinetic model was developed. [13]

1.6. **INFLUENCE OF WATER**

The reaction rate can be inhibited by the reverse reaction, dilution effects of liquid-phase systems, or when water is a product in reactions catalyzed by cation exchange resins. It is known that the last one inhibits the reaction rate much more than the other two. The inhibiting effect of water is due to its preferential association with sulfonic groups over catalysts.

This effect must be included in kinetic models and it complicates them especially when the reaction rate must be predicted over a wide concentration range. In order to quantify this effect, researchers use empirical inhibition factors in rate expression or choose to study the reaction in a specific concentration range.

The common approach to model the water inhibition effect is to express the rate constant as a function of the fraction of available active sites. The fraction of acid sites blocked by water molecules can be expressed by an adsorption isotherm. Some factors derived from Langmuir and Freundlich adsorption isotherms can be proposed. This is developed in the section "Development of mathematical models ".[14,15,16].

2. OBJECTIVES

The goal of the present study is to develop a kinetic model for 5-nonanol dehydration over Amberlyst45, for what is necessary to propose a set of kinetic equations with a mechanistic base. Following, the proposed models are fitted to the experimental data by computational tools. Then, the selection of the best model based on statistical and thermodynamical criteria will take place. Finally, we will add the influence of water to the best model to deduce if this term makes models better. The thermodynamical sense of water inhibition expression will be also discussed.

3. ANALYSIS OF REACTION RATES ON ACTIVITIES.

The experimental data has been provided by the "Applied kinetics and Catalysis" research group. The data consist of the activities of each component, the reaction rate, and the temperature at which the experiment was carried out. The explored temperature range varies from 413 to 453 K. The experimental data has been obtained using dioxane as a solvent to ensure a monophasic system since nonanol and nonenes are immiscible in water.

Figures 6,7,8 and 9 shows the dependence of reaction rates as a function of activities 5-nonanol (a_{NOH}), nonenes(a_N), water(a_W), and dioxane(a_D), respectively.

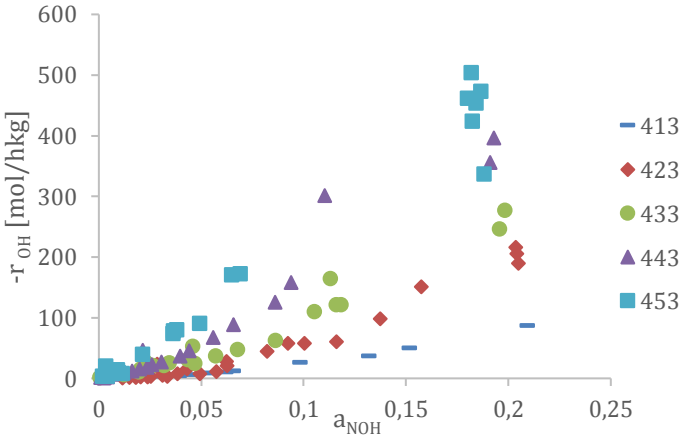

Figure 6 Dependence of reaction rates as a function of 5-nonanol activities.

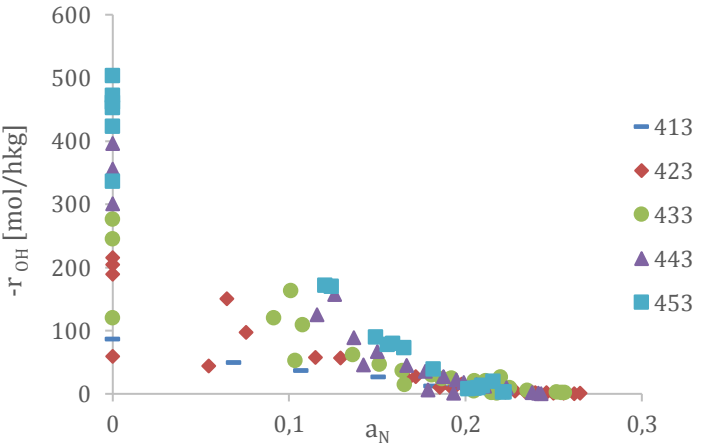

Figure 7 Dependence of reaction rates as a function of nonenes activities.

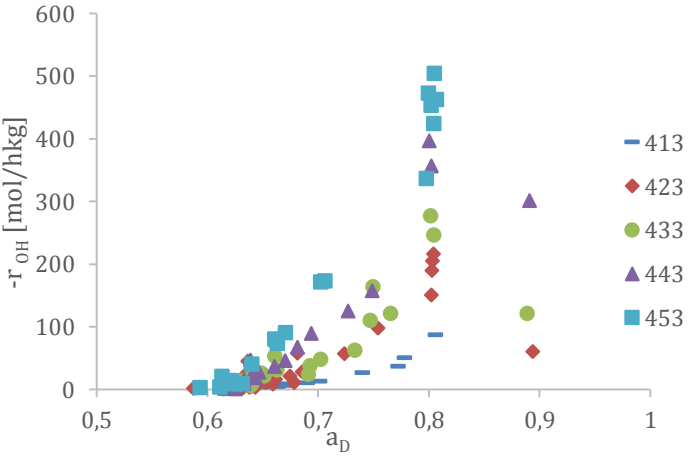

Figure 8 Dependence of reaction rates as a function of water activities

.

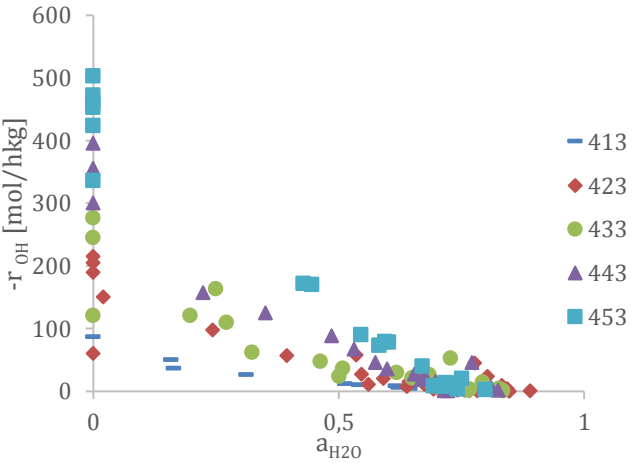

Figure 9 Dependence of reaction rates as a function of dioxane activities.

Figures 6, 7, 8, and 9 show that reaction rate is highly dependent on temperature. Furthermore, the reaction rate tends to zero when 5-nonanol activity is zero, this means the reaction is irreversible.

Due to de fact that a_{NOH} a_N and a_W are not independent variables, it is difficult to analyze the influence of each activity on the reaction rate. However, the reaction rate increases on increasing a_{NOH} in the entire range of explored activities and temperatures, whereas it decreases on increasing a_N and a_W. These facts suggest that a hyperbolic model, based on LHHW (equation 1) could satisfactorily explain rate data. The rate-decreasing effect showed by a_W can be attributed to preferential adsorption onto the resin, and also, as water is a reaction product due to system reaches its maximum conversion.

Figures 10, 11, 12, and 13 show the dependence of activities on temperatures. In all the figures, a gap is observed in the experimental data that is associated with a high reaction rate for each temperature, this is probably due to difficulties in the experimental procedure. In addition, this gap increases with increasing temperature. Therefore, experimental points are less dispersed for high-temperature values than for low-temperature values. The dioxane activity does not vary in relation to the temperature since it is the solvent.

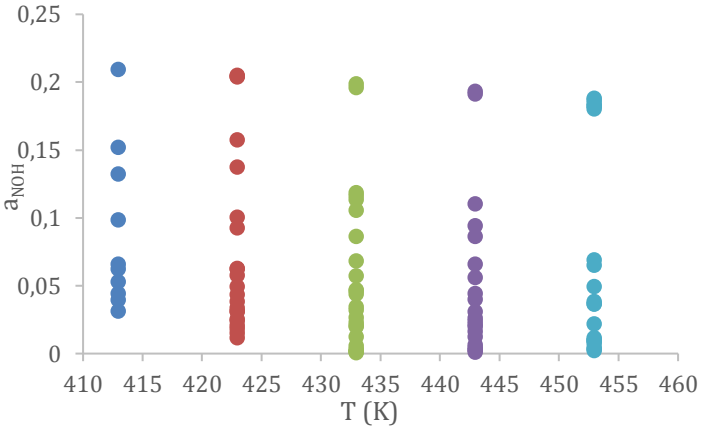

Figure 10 Dependence of 5-nonanol activities on temperatures.

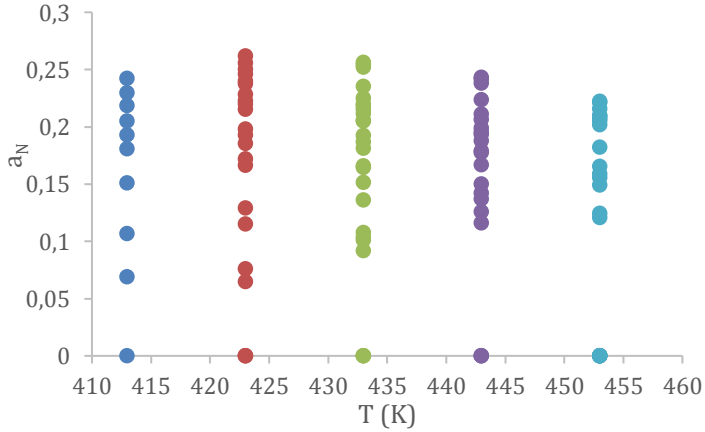

Figure 11 Dependence of nonene activities on temperatures.

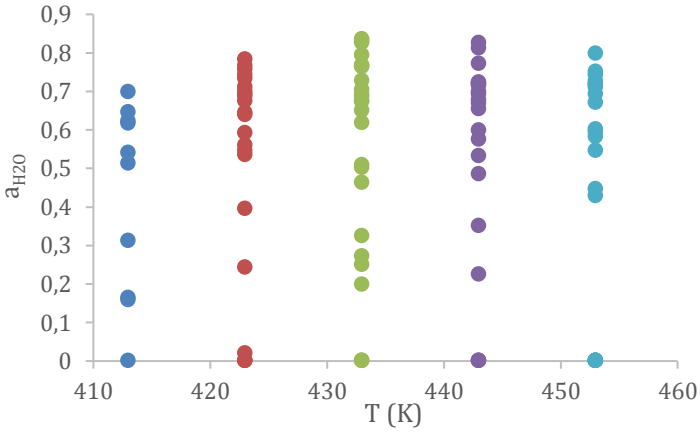

Figure 12 Dependence of water activities on temperatures.

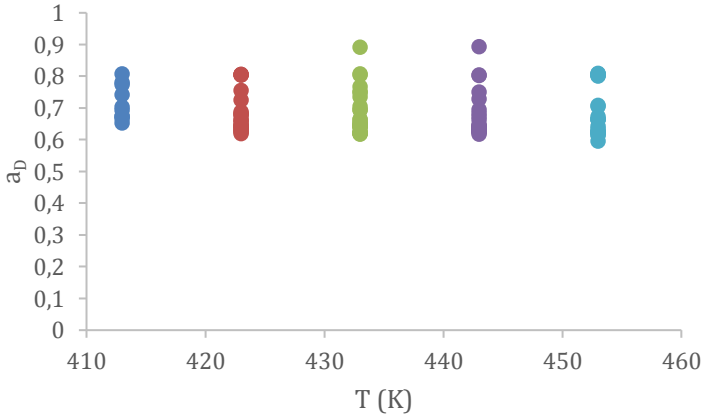

Figure 13 Dependence of dioxane activities on temperatures.

4. DEVELOPMENT OF MATHEMATICAL MODELS.

The reaction rate models considered in this work are based on the Langmuir-Hinshelwood-Hougen-Watson (LHHW). The three terms of the general kinetic equation 1 are derived. For this, a reaction mechanism is proposed for each step, the reaction on the surface is considered the determining step and the rest of steps are considered to be in a quasi-steady state.

Experimental data have been obtained with sufficient agitation to allow external mass transfer to be neglected. In addition, sufficiently small particle sizes have been used to neglect the internal mass transfer. Due to these two simplifications of mass transport phenomena, the external and internal transfer steps are not included in the proposed mechanism.

Elementary steps of the reaction mechanism:

The elementary steps are shown in the following expressions, in which σ represents an active site and NOH, N and H_2O correspond, respectively, to 5-nonanol, nonene, and water.

Nonanol adsorption

$$NOH + \sigma \rightleftharpoons NOH\sigma$$

Surface reaction

$$NOH\sigma + \sigma \rightarrow N\sigma + H_2O\sigma$$

Desorption products

$$N\sigma \rightleftharpoons \sigma + N$$

$$H_2O\sigma \rightleftharpoons \sigma + H_2O$$

The developed kinetic expressions derived from these steps are based on 3 assumptions:

- The number of surface active sites is constant.

- All the active sites are identical.

-The active sites reactivity does not depend on quantity and nature of the rest of compounds present on the solid surface during the reaction, it only depends on temperature.

Rate step expressions

Nonanol adsorption

$$r'_{ads,NOH} = k_{a,NOH}\, C_{NOH} \hat{C}_v - k_{d,NOH}\, \hat{C}_{NOH} \quad [2]$$

- $r'_{ads,NOH}$: Net adsorption rate.
- $k_{a,NOH}$: Adsorption rate constant.
- $k_{d,NOH}$: Desorption rate constant.
- C_{NOH}: Liquid phase concentration of nonanol.
- $\hat{C}_v$: Concentration of the empty sites on the catalyst surface.
- $\hat{C}_{NOH}$: Concentration of nonanol adsorbed.

The rate of adsorption is zero at equilibrium, from which the equilibrium adsorption constant is obtained.

$$0 = k_{a,NOH}\, C_{NOH} \hat{C}_v - k_{d,NOH}\, \hat{C}_{NOH} \quad [3]$$

$$K_{NOH} = \frac{k_{a,NOH}}{k_{d,NOH}} = \left[\frac{\hat{C}_{NOH}}{C_{NOH}\hat{C}_v}\right]_{eq} \quad [4]$$

Equation 2 can be rewritten taking into account expression 4 as

$$r'_{ads,NOH} = k_{a,NOH}\, C_{NOH} \hat{C}_v - \frac{k_{a,NOH}}{k_{a,NOH}/k_{d,NOH}} \hat{C}_{NOH} = k_{a,NOH} \left(C_{NOH} \hat{C}_v - \frac{\hat{C}_{NOH}}{K_{NOH}} \right)$$

Surface reaction:

$$r'_s = \hat{k}\, \hat{C}_{NOH} \hat{C}_v \quad [5]$$

Where $\hat{k}$ is the surface rate constant and r'_s is the surface reaction rate.

Desorption products

$$r'_{d,NO} = k_{d,N}\, \hat{C}_N - k_{a,NO}\, C_N \hat{C}_v \quad [6]$$

$$r'_{d,\,H_2O} = k_{d,H_2O}\, \hat{C}_{H_2O} - k_{a,H_2O}\, C_{H_2O} \hat{C}_v \quad [7]$$

- $r'_{d,N}$: Net desorption rate of nonene.
- $r'_{d,\,H_2O}$: Net desorption rate of water.
- $k_{d,N}$ Nonene desorption rate constant.

- k_{d,H_2O} Water desorption rate constant.
- $k_{a,N}$: Nonene adsorption rate constant.
- k_{a,H_2O} : Water desorption rate constant.
- C_N Liquid phase concentration of nonene.
- $\hat{C}_N$ Concentration of nonene adsorbed
- $\hat{C}_{H_2O}$ Concentration of water adsorbed
- C_{H_2O} Liquid phase concentration of water

Following the same procedure as mentioned above, the desorption rate of each product is obtained

$$0 = k_{d,N}\,\hat{C}_{NO} - k_{a,NO}\,C_N\hat{C}_v \qquad [8]$$

$$K_N = \frac{k_{a,N}}{k_{d,N}} = \left[\frac{\hat{C}_N}{C_N\,\hat{C}_v}\right]_{eq} \qquad [9]$$

$$0 = k_{d,H_2O}\,\hat{C}_{H_2O} - k_{a,H_2O}\,C_{H_2O}\hat{C}_v \qquad [10]$$

$$K_{H_2O} = \frac{k_{a,H_2O}}{k_{d,H_2O}} = \left[\frac{\hat{C}_{H_2O}}{C_{H_2O}\hat{C}_v}\right]_{eq} \qquad [11]$$

$$r'_{d,N} = \frac{k_{a,N}}{k_{a,N}/k_{d,N}}\hat{C}_N - k_{a,N}\,C_N\hat{C}_v \qquad [12]$$

$$r'_{d,N} = k_{a,N}\left(\frac{\hat{C}_N}{K_N} - C_N\,\hat{C}_v\right) \qquad [13]$$

$$r'_{d,\,H_2O} = k_{a,H_2O}\left(\frac{\hat{C}_{H_2O}}{K_{H_2O}} - C_{H_2O}\,\hat{C}_v\right) \qquad [14]$$

Obtaining the kinetic model considering one controlling step.

The controlling step is considered to be the surface reaction, so the surface reaction is assumed to be the slowest step. The overall rate is equal to equation 5.

If the reaction at the surface is the slowest stage, the adsorption of the reactant and the desorption of the products are in pseudo-equilibrium. This allows obtaining the concentration on the active centers as a function of the concentration in the fluid phase.

Nonanol adsorption

$$\left[k_{a,NOH}\left(C_{NOH}\hat{C}_v - \frac{\hat{C}_{NOH}}{K_{NOH}}\right)\right] \longrightarrow 0 \Rightarrow \hat{C}_{NOH} \approx K_{NOH}\, C_{NOH}\, \hat{C}_v \qquad [15]$$

Desorption products

$$\left[k_{a,N}\left(\frac{\hat{C}_{NO}}{K_{NO}} - C_{NO}\,\hat{C}_v\right)\right] \longrightarrow 0 \Rightarrow \hat{C}_N \approx C_N\,\hat{C}_v\,K_N \qquad [16]$$

$$\left[k_{a,H_2O}\left(\frac{\hat{C}_{H_2O}}{K_{H_2O}} - C_{H_2O}\,\hat{C}_v\right)\right] \longrightarrow 0 \Rightarrow \hat{C}_{H_2O} \approx C_{H_2O}\,\hat{C}_v K_{H_2O} \qquad [17]$$

Replacing equations 15, 16 and 17 in the total number of active centers, the concentration of empty active centers on the surface can be obtained as a function of the concentration of the species in the fluid phase.

$$\hat{C}_0 = \hat{C}_v + \hat{C}_{H_2O} + \hat{C}_N + \hat{C}_{NOH} \quad [18]$$

$$\hat{C}_0 = \hat{C}_v + C_{H_2O}\,\hat{C}_v K_{H_2O} + C_{NO}\,\hat{C}_v\,K_N + K_{NOH}\,C_{NOH}\,\hat{C}_v \qquad [19]$$

$$\hat{C}_v = \frac{\hat{C}_0}{1+C_{H_2O}\,K_{H_2O}+C_N\,K_N+K_{NOH}\,C_{NOH}} \quad [20]$$

Replacing equations 15 and 20 in equation 5, the expression of the reaction rate is obtained as a function of the concentration of the species of the fluid phase.

$$r' = r_s' = \hat{k}\,K_{NOH}\,C_{NOH}\left(\frac{\hat{C}_0}{1+C_{H_2O}\,K_{H_2O}+C_{NO}\,K_N+K_{NOH}\,C_{NOH}}\right)^2 \qquad [21]$$

$$r' = \hat{k}\,K_{NOH}\hat{C}_0{}^2\,\frac{C_{NOH}}{\left(1+C_{H_2O}\,K_{H_2O}+C_{NO}\,K_N+K_{NOH}\,C_{NOH}\right)^2} \qquad [22]$$

If the reacting mixture is assumed to be non-ideal, activities should be used instead of concentrations in the rate expression. Also "n" is included to obtain the most general expression for the rate of reaction, considering that 1,2 or 3 actives centers could be involved in the reaction.

$$r' = \frac{\hat{k}\,K_{NOH}\hat{C}_0{}^2 a_{NOH}}{\left(1+K_{H_2O}\,a_{H_2O}+K_N\,a_N+K_{NOH}\,a_{NOH}\right)^n} \qquad [23]$$

This general equation was fit to experimental data. Further, other derived equations have been considered. Models proposed have been modified by:

- Considering the number of active sites unoccupied negligible, eliminating the "1+" term from the equation.
- Number of active sites "n" were evaluated between 1 and 3.
- A summand is removed from the adsorption term when the adsorption of one compound on the catalyst is considered negligible
- Addition of the solvent (dioxane) in adsorption term.
- Addition of factor that considers water inhibition.

Additional factor to consider inhibition by water.

The correction factor presented below derives from the Freundlich isotherm. This correction factor has been chosen among those present in the literature because it presents better results. The inhibition factor $\eta(a_{H_2O})$ is dependent on the activity of water and temperature, it has to tend to 1 for the case of the absence of water. And usually should be considered as empirical rather than with a thermodynamical basis.[17-20]

$$\eta(a_{H_2O}) = \left(1 - K_W\, a_{H_2O}{}^{\frac{1}{\alpha}}\right)^n \quad [24]$$

Where $\alpha = \frac{K_\alpha}{T}$ and n are the sites taking part in the rate-limiting step.

$$K_W = \frac{K_{W1}}{T} exp\left[-K_{W2}\left(\frac{1}{T} - \frac{1}{T_{ref}}\right)\right] \quad [25]$$

A non-linear optimization method based on the Levenberg-Marquardt algorithm was used to fit the kinetic parameters by minimizing the sum of squared relative errors (SSRR). The algorithm has been implemented in Matlab.

The sum of normalized squared errors is defined as:

$$SSRR = \sum_i^N \left(\frac{r_{exp} - r_{cal}}{r_{exp}}\right)_i^2 \quad [26]$$

The kinetic constant and the adsorption constants depend on the temperature. The kinetic constant is described by the Arrhenius law (equation 27) and the adsorption constants by the van't Hoff law (equation 28).

$$\hat{k} = A\, exp\left[\frac{-E_a}{R}\left(\frac{1}{T} - \frac{1}{T_{ref}}\right)\right] \quad [27]$$

$$K_j = exp\left[\frac{\Delta S_j}{R} - \frac{\Delta H_j}{R}\left(\frac{1}{T} - \frac{1}{T_{ref}}\right)\right] \qquad [28]$$

The inverse of the reference temperature is the mean temperature and has been included to reduce the correlation between ΔH_j and ΔS_j in the fitting procedure.

To avoid overparameterization in the model fitting, rate and adsorption constant were grouped. How the groupings are made depends on each model. Apparent rate constant can associate rate constant, total active sites, and other adsorption constant if is convenient for fitting purpose. Parameters K_j can correspond to the actual adsorption equilibrium constant of each species or a combination of them. Equation 29 shows an example of how the constant association was made for the LHHW7 model.

$$r' = \frac{K_1 a_{NOH}}{(K_2 a_{H_2O} + K_3 a_{NO} + a_{NOH})^n} \qquad [29]$$

$$K_1 = \hat{k}\,\hat{C}_0^{\,2} \qquad [30]$$

$$K_2 = \frac{K_{H_2O}}{K_{NOH}} \qquad [31]$$

$$K_3 = \frac{K_{NO}}{K_{NOH}} \qquad [32]$$

In this case, four groups have been formed, which are related to temperature from the van't Hoff equation. What determines that this model has 8 parameters to fit from which the thermodynamic data can be obtained.

$$K_1 = exp\left[b_1 + b_2\left(\frac{1}{T} - \frac{1}{T_{ref}}\right)\right] \qquad [33]$$

$$K_2 = exp\left[b_3 + b_4\left(\frac{1}{T} - \frac{1}{T_{ref}}\right)\right] \qquad [34]$$

$$K_3 = exp\left[b_5 + b_6\left(\frac{1}{T} - \frac{1}{T_{ref}}\right)\right] \qquad [35]$$

$$K_4 = exp\left[b_7 + b_8\left(\frac{1}{T} - \frac{1}{T_{ref}}\right)\right] \qquad [36]$$

For the sake of clarity, b_1 allows obtaining an apparent pre-exponential factor while b_2 an apparent energy activation. From b_3 and b_4 reaction entropy and enthalpy. However, b_5 allows to obtain the difference between water and nonanol entropy, and b_6 the difference between water and nonanol enthalpy adsorption. Analogously, must proceed with b_7 and b_8. [17,18]

5. RESULTS AND DISCUSSION

Criteria for model selection

Considering the different forms of the adsorption term, a total of 85 equations have been obtained to evaluate. Three groups of models have been made for their correct analysis. The first group includes models 1 to 10 presented in table 15 of the appendix 1. In which the influence of the solvent and the inhibition by water are not considered. The second group includes models 11 to 25 and are a modification of the first group adding the influence of the solvent. The last group contemplates inhibition by water.

An adequate model must accurately predict the results of each experiment. In addition, the values of the estimated parameters must present a coherent thermodynamic and kinetic meaning. To discriminate between the different kinetic models, several criteria have been adopted. Consequently, the models with the highest sum of squared relative error (SSRR)(equation 43) are first discarded. Then, the error of the parameters and their correlation will be analyzed, and finally, those models whose parameters do not make thermodynamic sense will be discarded. The randomness of the residual error will also be analyzed.

Evaluation by the sum of squared relative errors

From a mathematical point of view, the most suitable model is the one with the smallest RSSQ, as this is a measure of the difference between prediction and experimental data.

The relative error is used instead of the residual error to obtain a good fit in all prediction range.[18]

To make a proper comparison between the models, the quotient between the minimum error of the group of models analyzed and the error of each model has been represented. The values closest to 1 will represent the best models, since they will have the smallest deviations. Figure 14 shows the results of the first group.

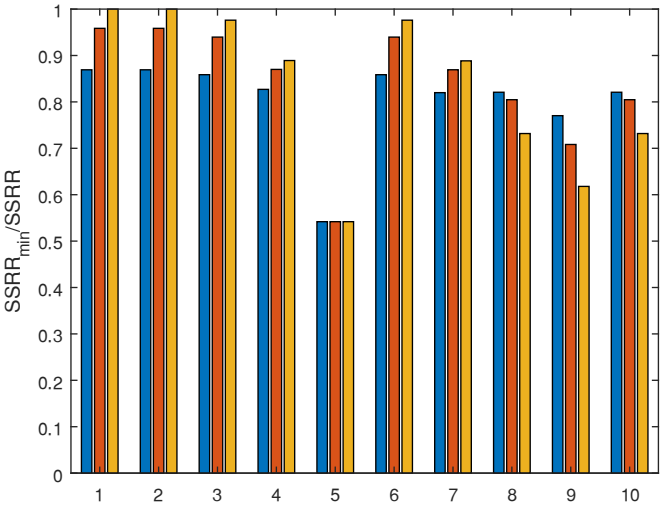

Figure 14 Comparison group 1 in terms of SSRRmin/SSRR.

Of this first group, model 5 is discarded since it presents a greater error. Carrying out a visual inspection, it is considered to discard models with a value lower than 0.8. Then, models 8 (n=3), 9 (n=1,2,3), 10 (n=3) are rejected.

A trend is observed regarding the number of active centers involved in the reaction on the surface. Models 1 to 7 contemplate the term "+1" in the adsorption group. This group shows a lower error when the number of active centers involved in the limiting step is 3. While models 8 to 10 show a lower error when the number of active centers involved in the limiting step is 1.

Second group is represented in figure 15. Models 15, 23 and 25 are discarded since they have a higher error. Then, following the same criteria as mentioned above, models 13(n=1), 16(n=1), 20(n=1), 23 (n=1) are discarded, given that the quotient is less than 0, 8. A better fit is obtained with 3 as the number of active centers involved in the surface reaction for all models.

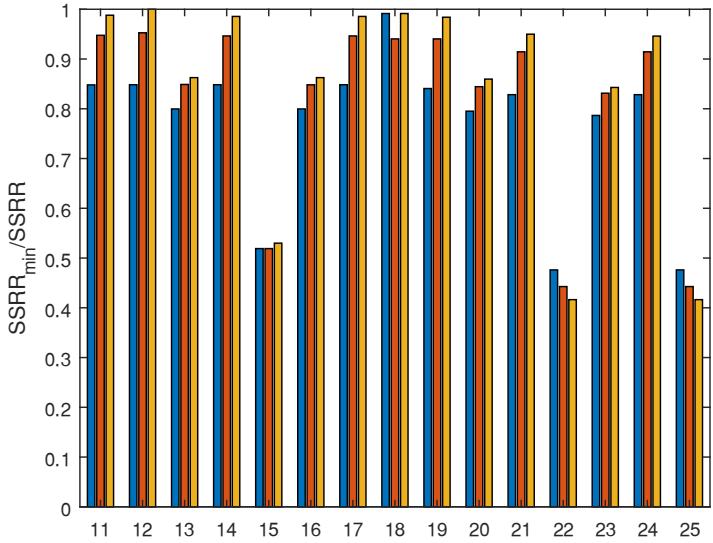

Figure 15 Comparison group 2 in terms of SSRRmin/SSRR.

Group 1 is compared with group 2 in a single graph (figure 16) to assess whether adding the solvent (dioxane) to the model significantly improves the fit. The minimum SSRR taken as reference corresponds to the minimum of the set formed by both groups.

Figure 16 shows an improvement in the fit in the models where the solvent has been added in the adsorption term, however, the improvement is not significant. Similar values of SSRR were obtained for group 1 and group 2.

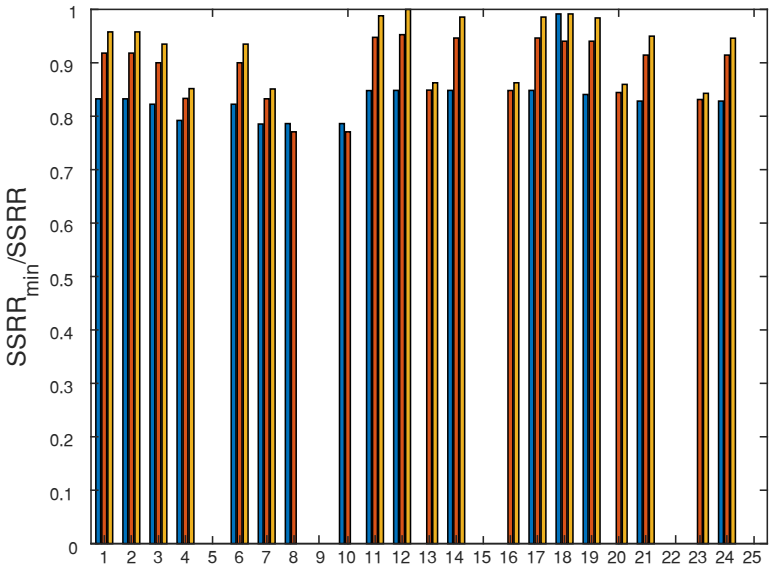

Figure 16 Comparison group 1 and 2 in terms of SSRRmin/SSRR.

Parameter error

The error value of the parameter has been estimated as the Standard deviation, this is the square root of the diagonal elements of the covariance matrix of the parameter estimates. The covariance matrix is defined by the equation 37.

$$V(b) = s^2(X^T * X)^{-1} \qquad [37]$$

Where $V(b)$ is the covariance matrix, s is the calculated fit error variance and X is Jacobian (a matrix of sensitivities).

Parameter standard deviations (sb_j) are measures of parameter uncertainty and have the same units as do the parameter values (bj). However, the ratio between confidence intervals (ε_j) and its parameter values is a better measure for comparison as is related to the parameter size.

The criterion taken to analyze the error of the parameter consists of discarding all the models that have some parameter with a ratio equal or greater than 1, as those parameters are very likely nonsignificant. Ratios values closer to 0 indicates that the parameter value is much bigger than its confidence interval, these parameters are preferable. Table 1 shows each model and its ratio. Confidence intervals have been calculated for a 95%-probability level.

Table 1 Comparison between parameters and its confidence interval LHHW 2,4 and 6

LHHW	2	2	2	4	4	4	6	6	6
n	1	2	3	1	2	3	1	2	3
ε_1/b_1	0,07	0,09	0,09	0,05	0,06	0,06	0,03	0,02	0,02
ε_2/b_2	-0,80	-0,76	-0,70	-0,72	-0,72	-0,67	-0,34	-0,31	-0,29
ε_3/b_3	0,25	0,34	0,43	0,35	1,03	-2,04	0,12	0,14	0,18
ε_4/b_4	2,98	4,03	4,84	1,68	0,62	0,58	0,52	0,49	0,48
ε_5/b_5	-8,55	-5,44	-4,11	-121619	-24,64	-24,97			
ε_6/b_6	-5,19	-3,14	-2,55	-117589	29,25	32,33			
ε_7/b_7									
ε_8/b_8									

Table 2 Comparison between parameters and its confidence interval LHHW 7,10, 12, and 13

LHHW	7	7	7	10	10	12	12	13
n	1	2	3	1	2	2	3	2
ε_1/b_1	4,05	4,19	4,25	0,04	0,07	2,93	3,09	3,26
ε_2/b_2	0,00	0,00	0,00	-0,33	-0,28	6,68	6,20	10,79
ε_3/b_3	12,47	69,74	-166,21	0,26	0,69	4,82	4,31	6,67
ε_4/b_4	1,26E-07	2,30E-07	2,90E-07	0,84	8,49	5,66	5,53	7,87
ε_5/b_5						5,26	4,60	-310,46
ε_6/b_6						7,39	6,93	-71,53
ε_7/b_7						3,63	3,49	5,76
ε_8/b_8						5,50	5,47	6,68

Table 3 Comparison between parameters and its confidence interval LHHW 16,18, 19, and 20

LHHW	16	16	18	18	19	19	19	20	20
n	2	3	1	3	1	2	3	2	3
ε_1/b_1	1,70	1,82	0,93	0,68	1,22	0,84	0,74	2,45	1,92
ε_2/b_2	5,59	5,52	5,04	1,54	5,33	2,41	1,57	5,00	3,46
ε_3/b_3	3,91	4,22	-13,65	-1,62	8,37	7,45	5,92	5,53	4,18
ε_4/b_4	3,75	3,24	-20,95	1,94	2,94	1,38	0,99	4,13	2,81
ε_5/b_5	3,19	3,68	11,75	9,62	2,51	1,37	1,01	4,52	3,70
ε_6/b_6	3,27	2,76	2,25	0,94	2,99	1,57	1,17	3,93	2,78
ε_7/b_7			2,11	1,01					
ε_8/b_8			2,31	1,17					

Table 4 Comparison between parameters and its confidence interval LHHW 21,23 and 24.

LHHW	21	21	21	23	23	24	24	24
n	1	2	3	2	3	1	2	3
ε_1/b_1	160289	26812	0,94	0,04	0,04	0,03	0,06	0,08
ε_2/b_2	-1858897	-195453	-5,25	-0,18	-0,20	-0,16	-0,19	-0,21
ε_3/b_3	209685	29564	1,65	-0,46	5,49	-0,12	-0,11	-0,12
ε_4/b_4	899650	-289970	-6,33	-0,43	-0,42	-0,50	-0,46	-0,46
ε_5/b_5	188910	28245	1,26					
ε_6/b_6	343840	-1036928	-9,99					
ε_7/b_7								
ε_8/b_8								

Models 1,3,8,9, 11, 12(n=1), 13(n=3) 14, 17,18 have been discarded and therefore, are not included in table 1 to 4. In those fitted models was noted that the implied b_1 is very negative. This means that the apparent constant (k') is practically 0. It indicates that the optimal value of k' would be negative, however k' could not be negative for kinetics models. Then adding this k' does not imply an improvement of the fit.

After analyzing tables 1 to 4, the possible candidates are models 6, 10 (n=1), 23 (n=2) and 24 since they meet the criteria.

Correlation matrix

Correlation coefficients parameter (pcc) are calculated as the covariance (cov) between two parameters divided by the product of their standard deviations (equation 38). Whether the non-diagonal absolute values are closer to zero means less correlation between parameters. However, unique values are nearly always assured if the absolute values of all pcc are all less than about 0.95.

$$pcc(j,k) = \frac{cov(j,k)}{var(j)^{1/2}\, var(k)^{1/2}} \quad [38]$$

Where j and k represent two parameters.

Table 5 show the covariance matrix of the 6,10, 23 and 24 LHHW models. Only model 24(n=3) has a parameter with pcc equal to 0.95, however it will be considered. Since all the rest pcc values are lower than 0.95 no model is discarded. Then, the correlation between parameters is not significant.

Table 5 Cross-correlation matrices of LHHW 6,10 and 23

LHHW	n	Cross-correlation matrices			
6	1	1,00	0,29	0,86	0,08
		0,29	1,00	0,13	0,82
		0,86	0,13	1,00	-0,09
		0,08	0,82	-0,09	1,00
6	2	1,00	0,25	0,84	-0,01
		0,25	1,00	0,05	0,78
		0,84	0,05	1,00	-0,24
		-0,01	0,78	-0,24	1,00
6	3	1,00	0,23	0,83	-0,04
		0,23	1,00	0,02	0,77
		0,83	0,02	1,00	-0,29
		-0,04	0,77	-0,29	1,00
10	1	1,00	0,36	0,89	0,31
		0,36	1,00	0,32	0,88
		0,89	0,32	1,00	0,31
		0,31	0,88	0,31	1,00
23	2	1,00	-0,25	0,90	-0,20
		-0,25	1,00	-0,20	0,92
		0,90	-0,20	1,00	-0,10
		-0,20	0,92	-0,10	1,00
24	1	1,00	-0,21	0,76	-0,16
		-0,21	1,00	-0,18	0,80
		0,76	-0,18	1,00	-0,01
		-0,16	0,80	-0,01	1,00
24	2	1,00	-0,26	0,90	-0,19
		-0,26	1,00	-0,20	0,91
		0,90	-0,20	1,00	-0,09
		-0,19	0,91	-0,09	1,00
24	3	1,00	-0,23	0,94	-0,17
		-0,23	1,00	-0,18	0,95
		0,94	-0,18	1,00	-0,10
		-0,17	0,95	-0,10	1,00

Coherence of thermodynamic and kinetic parameters

As it mentioned above, parameters b_1 and b_2 are related to the kinetic constant. Kinetic models where the obtained apparent activation energy is negative are discarded. Then b_2 must be negative.

Parameters b_3, b_5, b_7 are related to adsorption entropy while parameters b_4, b_6, b_8 are related to adsorption enthalpy. For a candidate model, their values, and taking into account the parameter uncertainty, have to fulfill the Boudart rules [14]:

(i) $\Delta S_j < 0$ because the adsorption process implies a loss of entropy.

(ii) $|\Delta S_j| < S_j$ because the loss of entropy cannot be larger than the total entropy.

(iii) $\Delta H_j < 0$ because adsorption is an exothermic process.

Table 6 Parameter and confidence interval for LHHW 6,10, 23 and 24

LHHW	n	b_1	ε_1	b_2	ε_2	b_3	ε_3	b_4	ε_4
6	1	7,1	0,2	-7330	2468	2,6	0,3	8273	4342
6	2	7,2	0,2	-7163	2200	1,5	0,2	6072	2992
6	3	7,2	0,2	-7123	2097	1,0	0,2	5369	2597
10	1	5,2	0,2	-8831	2889	1,0	0,3	4102	3462
23	2	6,0	0,2	-18285	3359	-0,4	0,2	-5747	2465
24	1	4,5	0,1	-14847	2312	-2,5	0,3	-7741	3893
24	2	3,7	0,2	-16817	3168	-1,5	0,2	-5031	2331
24	3	3,2	0,3	-18337	3919	-1,1	0,1	-3893	1802

The parameter b_2 has a negative sign for all the models present in table 6. Therefore, the apparent activation energy is positive.

The parameter b_3 is positive for model 6. Since in this model it represents the sign of the entropy, it should be negative to make thermodynamic sense. Then model 6 has not a mechanistic base, and therefore it could not be extrapolated to other operational conditions.

Parameter b_3 represents $\Delta S_N - \Delta S_{\mathrm{NOH}}$ for model 10, $\Delta S_D - \Delta S_{H_2O}$ for model 23 and $\Delta S_D - \Delta S_{\mathrm{N}}$ for model 24. Bigger molecules should have a greater loss of entropy.

Parameter b_4 represents $-(\Delta \mathrm{H_N} - \Delta \mathrm{H_{NOH}})$ for model 10, $-(\Delta H_D - \Delta H_{H_2O})$ for model 23 and $-(\Delta H_D - \Delta H_{\mathrm{N}})$ for model 24. Then, parameters model 10, 23 and 24 make

thermodynamic sense. By equation 34 and parameters values b_3 and b_4 adsorption ratios constant can be calculated at different temperatures to indicate which compound is preferable adsorbed. Estimated differences of adsorption enthalpies and entropies for each model are presented below.

Table 7 thermodynamic and kinetic parameters LHHW 10 (n=1)

A	$E'_a\ [kJ/mol]$	$\Delta S_N - \Delta S_{\mathrm{NOH}}\ [J/mol\,K]$	$\Delta H_N - \Delta H_{\mathrm{NOH}}\ [kJ/molK]$
186±1	73±24	8±2	-34±29

Results for model 10 indicate that nonene adsorption is more exothermic than nonanol adsorption and that the entropic loss for the adsorbed nonanol is larger than for the adsorbed nonene. This is consistent since nonanol is a larger molecule than nonene and the reduction in the rotation due to the double bond. Estimated K_N/K_{NOH} values ranged from 4,23 at 413K to 1,76 at 453 K. Such decrease suggests that nonene adsorption is losing relevance with temperature, compared to nonanol adsorption. On the contrary, since nonene is nonpolar, it should be less adsorbed on the resin than nonanol.

Table 8 thermodynamic and kinetic parameters LHHW 23 (n=2)

A	$E'_a\ [kJ/mol]$	$\Delta S_D - \Delta S_{H_2O}\ [J/mol\,K]$	$\Delta H_D - \Delta H_{H_2O}\ [kJ/molK]$
394±1	152±28	-3±1	-48±20

Results for model 23 indicate that dioxane adsorption is more exothermic than water adsorption and that the entropic loss for the adsorbed water is larger than for the adsorbed dioxane. Estimated K_D/K_{H2O} values ranged from 0,36 at 413K to 1,22 at 453 K. Water adsorption seems to be more favored than dioxane adsorption at low temperature, and less favored at high temperature. This agrees with the polarity of the molecules.

Table 9 thermodynamic and kinetic parameters LHHW 24 (n=1,2,3)

n	A	$E'_a\ [kJ/mol]$	$\Delta S_D - \Delta S_N\ [J/mol\,K]$	$\Delta H_D - \Delta H_N\ [kJ/molK]$
1	86±1	123±19	-21±2	64±20
2	40±1	140±26	-13±1	42±19
3	24±1	152±33	-9±1	32±15

Results for model 24 indicate that nonene adsorption is more exothermic than dioxane adsorption and that the entropic loss for the adsorbed dioxane is larger than for the adsorbed nonene. Estimated K_D/K_N values ranged from 0,04, 0,12 and 0,21 at 413K to 0,19, 0,36, 0,48 at

453 K, for n=1,2,3 respectively. Nonene adsorption seems to be more favored than dioxane adsorption in all the explored range of temperature. Dioxane absorption should be more favored by polarity.

Calculated reaction rates versus experimental reaction rates and residual error are represented in figure 17 to 22 to determine if one of these models is better than another one.

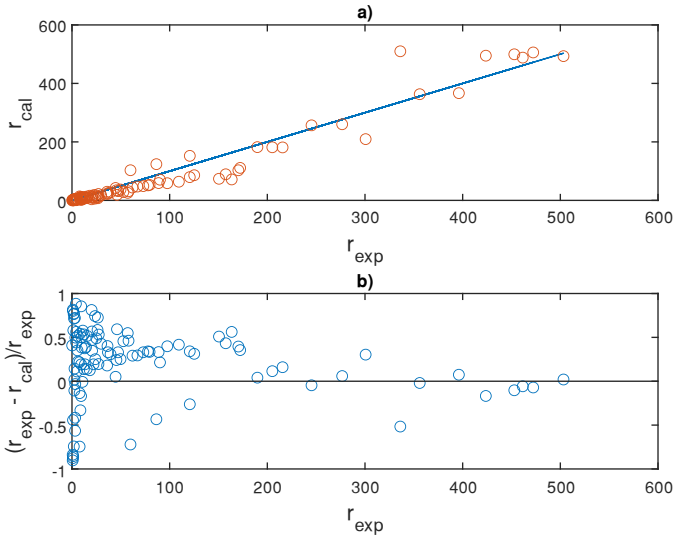

Figure 17 Calculated reaction rates versus experimental reaction rates and residual LHHW 6 n=3

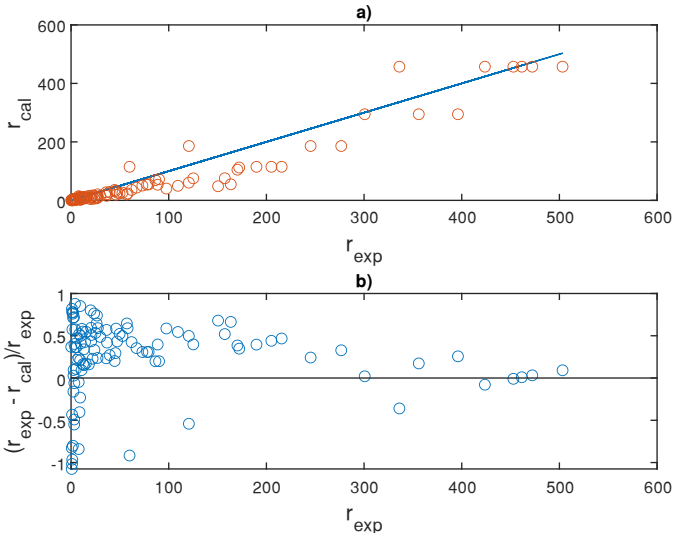

Figure 18Calculated reaction rates versus experimental reaction rates and residual LHHW 10 n=1

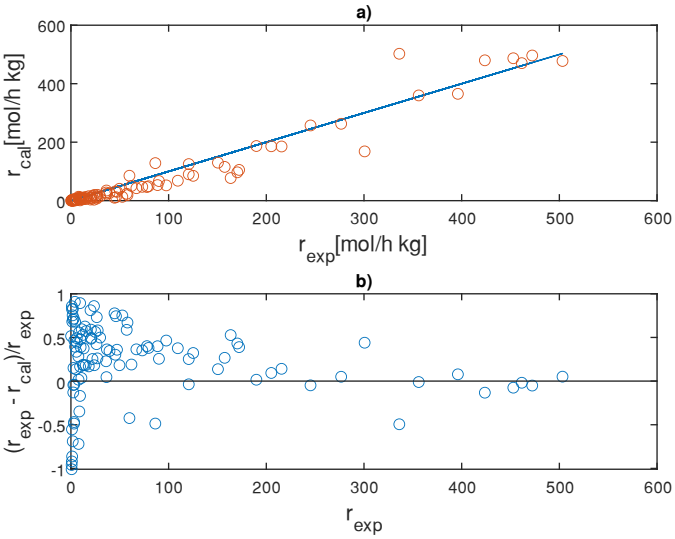

Figure 19 Calculated reaction rates versus experimental reaction rates and residual LHHW23 n=2

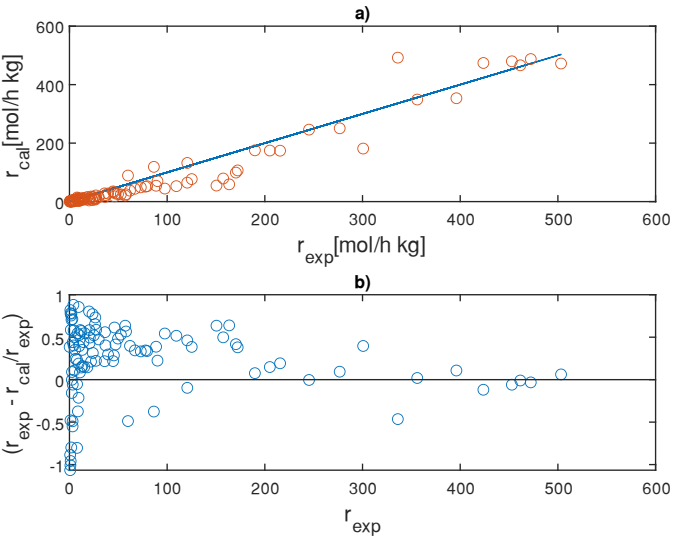

Figure 20 Calculated reaction rates versus experimental reaction rates and residual LHHW 24 n=1

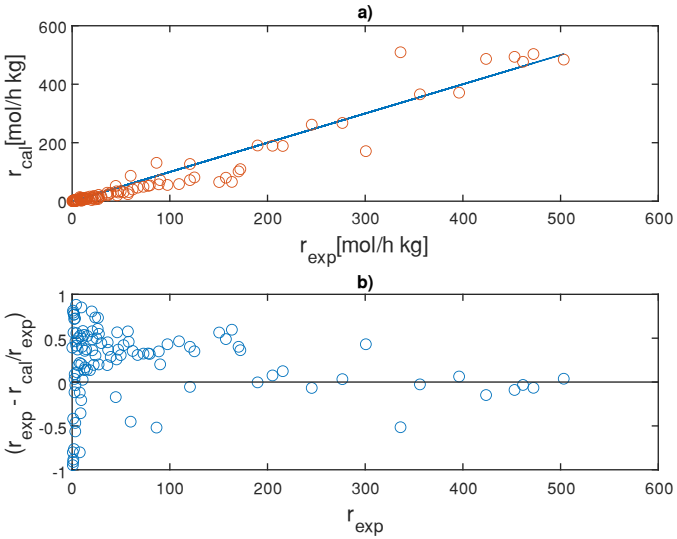

Figure 21 Calculated reaction rates versus experimental reaction rates and residual LHHW 24 n=2

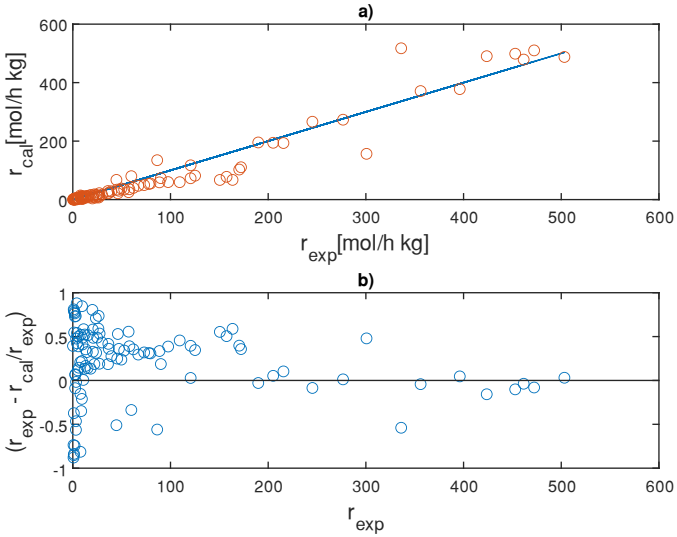

Figure 22 Calculated reaction rates versus experimental reaction rates and residual LHHW 24 n=3

Models 6, 10, 23 and 24 underestimate the experimental values for low values of reaction

rate. Therefore, the residual error is not random. For high reaction rate values, the residual error is random but the number of experimental points is smaller. As all models present similar behavior it is not possible to discriminate between them under these criteria.

Neither of models presents "+1" in adsorption terms. This fact suggests the number of active sites unoccupied can be considered negligible, what seems reliable in liquid-phase reactions catalyzed by solids.[20]

Finally, neither the relationship between the parameters and the confidence interval nor the correlation between the parameters reflect that one of these two models is better than the other. Then the SSRR is compared. Since model 24 (n=3) and 6(n=3) has lower SSRR, those are considered the best models from group 1 and 2. Model 24 has the advantage of having a mechanistic base, therefore it could be extrapolated in other operating conditions, while model 6 could not be extrapolated.

Addition of water inhibition term.

Following, the third group of fitting models is presented. This group adds a factor that considers water inhibition in models 6, 10, 23 and 24. Water adsorption term must be eliminated in the denominator to include water inhibition. Then model 23 is modified, leading to an expression similar to model 25. The mathematical expression for group 3 is presented in table 17 in the appendix.

Table 10. Model 6, 10 and 24 modified by the addition of water inhibition.

	LHHW 6-W			LHHW10-W	LHHW24-W		
n	1	2	3	1	1	2	3
ε_1/b_1	0,02	0,02	0,02	0,04	0,2	0,2	0,3
ε_2/b_2	-0,29	-0,28	-0,28	-0,27	-0,7	-0,8	-1,0
ε_3/b_3	1,14	1,14	1,85	905,97	-1,0	-0,7	-0,7
ε_4/b_4	2,97	3,73	3,76	-4,43	-2,7	-3,5	-4,2
$\varepsilon_{K_{W1}}/K_{W1}$	0,40	0,58	0,67	0,29	0,4	0,5	0,6
$\varepsilon_{K_{W2}}/K_{W2}$	-1,90	-1,41	-1,32	-2,11	-2,0	-1,4	-1,2
$\varepsilon_{K_\alpha}/K_\alpha$	1,22	0,91	0,89	1,70	1,3	0,9	0,9
SSRR	20,56	19,90	19,70	21,18	20,3	19,3	18,8
SSRR% variation	19,8	15,1	12,7	21,1	20,5	16,5	15,7

Table 11 Model 25-w modified by the addition of water inhibition

	LHHW25-W		
n	1	2	3
ε_1/b_1	0,03	0,03	0,03
ε_2/b_2	-0,23	-0,23	-0,23
$\varepsilon_{K_{W1}}/K_{W1}$	0,10	0,13	0,13
$\varepsilon_{K_{W2}}/K_{W2}$	-0,86	-0,80	-0,86
$\varepsilon_{K_\alpha}/K_\alpha$	0,41	0,32	0,29
SSRR	21,89	21,45	21,64
SSRR% variation	50,60	54,99	57,29

Table 10 and 11 shows SSRR% variation over each LHHW modified. SSRR decreases greatly. The fitting upgrade could be ascribed to the inclusion of a more adjustable parameter, or else that the Freundlich adsorption power-type expression for water is flexible enough to fit rate data properly. However, some parameters have associated confidence interval greater than the parameter value on models 6-W, 10-W and 24-W. Model 25-W show SSRR better improvement and has no interval confidence greater than the parameter value.

Figures 23, 24 and 25 show calculated reaction rates versus experimental reaction rates and residual error distribution for model 25-W. The same graphs are presented in figure 29 to 35 in the appendix 2 for model 6-W, 10-W and 24-W, respectively.

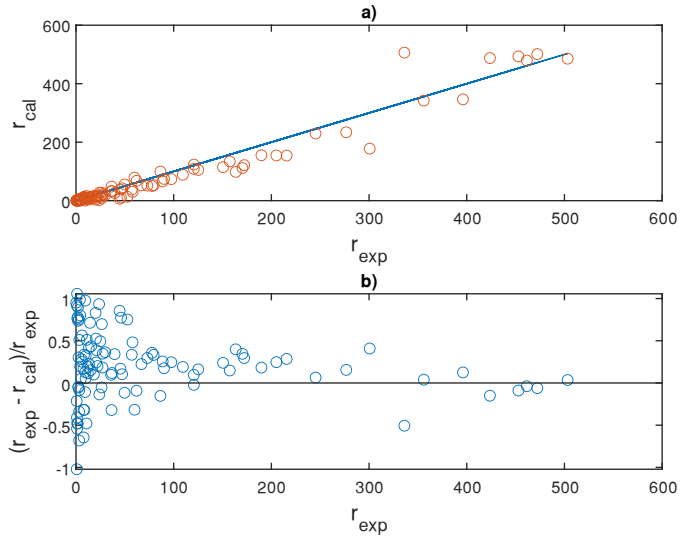

Figure 23 Calculated reaction rates versus experimental reaction rates and residual LHHW 25-W n=1

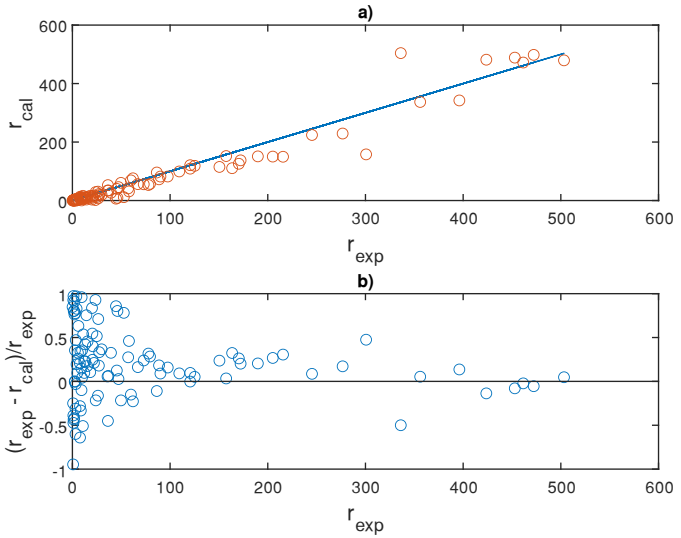

Figure 24 Calculated reaction rates versus experimental reaction rates and residual LHHW 25-W n=2

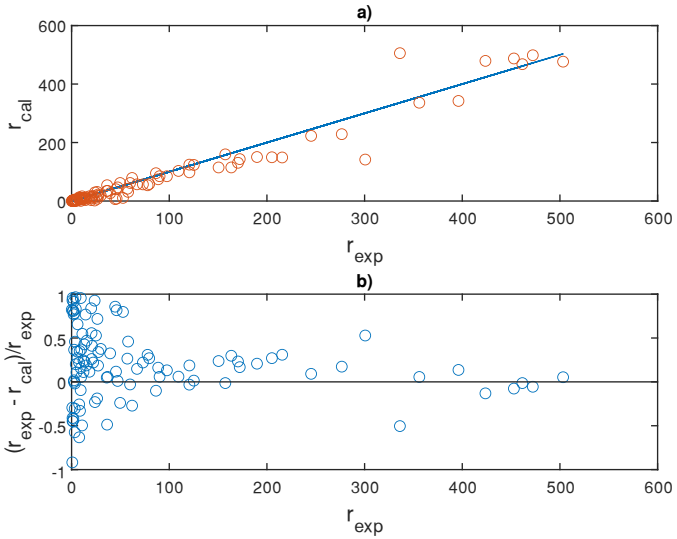

Figure 25 Calculated reaction rates versus experimental reaction rates and residual LHHW 25-W n=3

All models achieve better residual distribution but model 25-W presents better improvement. Taking into account both approaches simultaneously, the addition of the water inhibition term presents an improvement in fitted models but it should be applied to models with reduced adjustable number parameters otherwise leads to over parametrization. Following, table 12 shows correlation matrix.

Table 12 Cross-correlation matrices of LHHW25-W

n	Correlation matrix				
1	1,00	0,28	-0,39	0,20	0,72
	0,28	1,00	-0,49	-0,65	0,40
	-0,39	-0,49	1,00	0,40	-0,87
	0,20	-0,65	0,40	1,00	-0,04
	0,72	0,40	-0,87	-0,04	1,00
2	1,00	0,26	-0,33	0,05	0,68
	0,26	1,00	-0,39	-0,73	0,35
	-0,33	-0,39	1,00	0,36	-0,88
	0,05	-0,73	0,36	1,00	-0,15
	0,68	0,35	-0,88	-0,15	1,00
3	1,00	0,26	-0,29	-0,01	0,67
	0,26	1,00	-0,35	-0,75	0,33
	-0,29	-0,35	1,00	0,33	-0,87
	-0,01	-0,75	0,33	1,00	-0,18
	0,67	0,33	-0,87	-0,18	1,00

As no parameter has a correlation factor greater than 0,95, the correlation between parameters can be considered not significant. Then model 25-W is considered the best one of group 3. The results associated with the parameters and their confidence interval for the 25-W model are presented below.

Table 13 thermodynamic and kinetic parameters 25-W

n	A	E'_a[kJ/mol]	K_{W1}	K_{W2}	K_α
1	945±1	68±15	460±45	-894±765	489±198
2	743±1	67±15	460±53	-1173±944	313±102
3	594±1	68±16	360±45	-1091±936	289±83

The parameter b_2 makes thermodynamic sense since positive apparent activation energy has been obtained. The dependence of the water inhibition term on the water activity for each temperature is presented below in figures 26, 27 and 28. Inhibition factor (equations 24) could be looked as a result of a Freundlich adsorption isotherm for water if Kw and a decrease with temperature, and α >1.

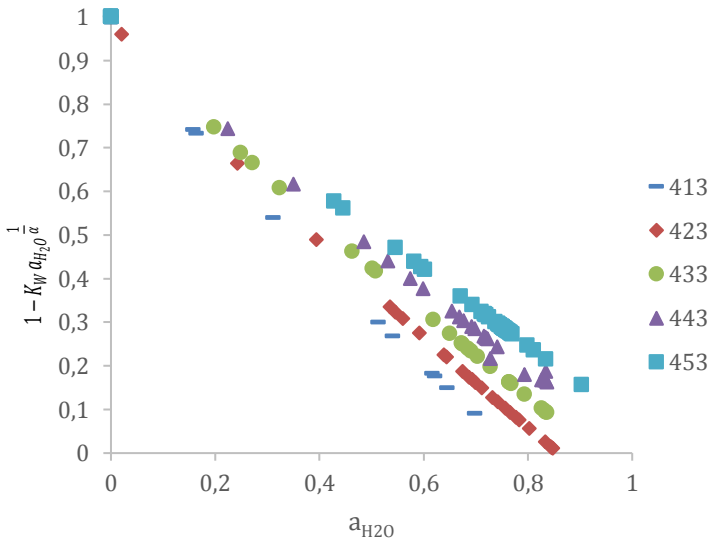

Figure 26 Correction factor versus a_w in the whole temperature for n=1

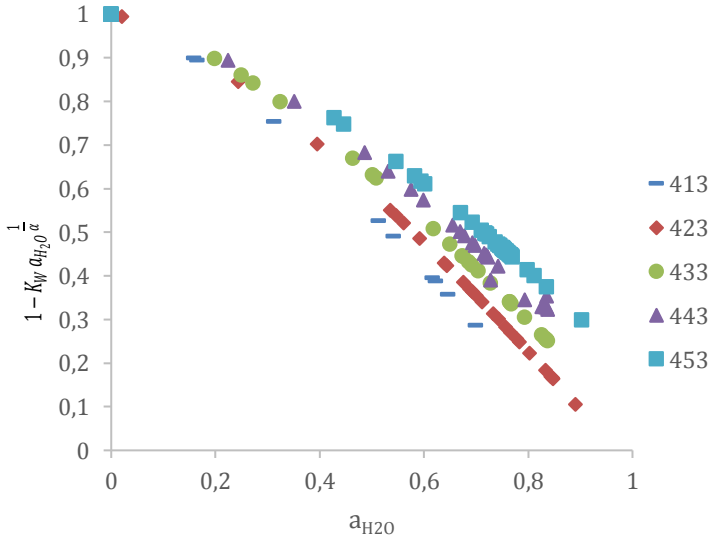

Figure 27 Correction factor versus a_w in the whole temperature range n=2.

.

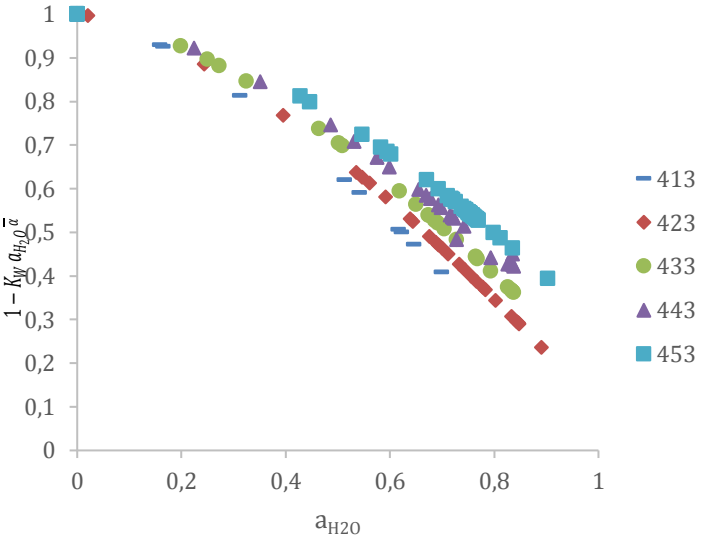

Figure 28 correction factor versus a_w in the whole temperature range n=3.

The inhibition factor decreases with temperature and decreases on increasing a_W for n=1,2,3. This agrees with the Freundlich adsorption isotherm. However, α values ranged from 1,19 to 1,10 for n=1, from 0,76 to 0,79 for n=2 and from 0,70 to 0,64 for n=3 at 413 to 453K, respectively. As $\alpha < 1$ for n=2 and 3, this correction factor should be considered empirical rather than with a thermodynamical basis, thus fitting improvement is probably due to the flexibility of the power expression (equation 24). Due to its pseudoempirical background the extrapolation to other operating conditions should be done with caution. While model 25-W has thermodynamical basis for n=1. Therefore it could be extrapolated. This result suggests that one active site is involved in the rate-limiting step.

The obtained apparent activation energy values could be compared with the existing values in the literature for the dehydration of other alcohols. For the dehydration of 1-octanol the apparent energy activation obtained was 120 ± 7 kJ / mol by Casas et al.(reff 18). For the dehydration of 1-Butanol to Di-n-butyl Ether over Amberlyst 70 the apparent energy activation obtained was 122± 62 kJ/mol by Pérez-Maciá et al.(reff 17). Table 14 shows thermodynamic and kinetic parameters of best models.

Table 14 Resume thermodynamic and kinetic parameters of best LHHW.

LHHW 10 (n=1)

$$r' = \frac{\hat{k}\,\hat{C}_0{}^2\,a_{NOH}}{\left(\frac{K_N}{K_{NOH}}a_N + a_{NOH}\right)^1}$$

SSRR=26,83

A	$E'_a\ [kJ/mol]$	$\Delta S_N - \Delta S_{NOH}\ [J/mol\ K]$	$\Delta H_N - \Delta H_{NOH}\ [kJ/molK]$
186±1	73±24	8±2	-34±29

LHHW 23 (n=2)

$$r' = \frac{\hat{k}\,\frac{K_{NOH}}{K_{H_2O}}\hat{C}_0{}^2\,a_{NOH}}{\left(a_{H_2O} + \frac{K_D}{K_{H_2O}}a_D\right)^2}$$

SSRR=25,38

A	$E'_a\ [kJ/mol]$	$\Delta S_D - \Delta S_{H_2O}\ [J/mol\ K]$	$\Delta H_D - \Delta H_{H_2O}\ [kJ/molK]$
394±1	152±28	-3±1	-48±20

LHHW 24 (n=1,2,3)

$$r' = \frac{\hat{k}\,\frac{K_{NOH}}{K_N}\hat{C}_0{}^2\,a_{NOH}}{\left(a_N + \frac{K_D}{K_N}a_D\right)^n}$$

$SSRR_{n=1}$=25,46 $SSRR_{n=2}$=23,06 $SSRR_{n=3}$=22,30

n	A	$E'_a\ [kJ/mol]$	$\Delta S_D - \Delta S_N\ [J/mol\ K]$	$\Delta H_D - \Delta H_N\ [kJ/molK]$
1	86±1	123±19	-21±2	64±20
2	40±1	140±26	-13±1	42±19
3	24±1	152±33	-9±1	32±15

LHHW 25-W (n=1,2,3)

$$r' = \hat{k}\,\frac{K_{NOH}}{K_D}\hat{C}_0{}^2\,a_{NOH}\left(\frac{1 - K_W\,a_{H_2O}{}^{\frac{1}{\alpha}}}{a_D}\right)^n$$

$SSRR_{n=1}$=21,89 $SSRR_{n=2}$=21,45 $SSRR_{n=3}$=21,64

n	A	E'a[kJ/mol]	K_{W1}	K_{W2}	K_α
1	945±1	68±15	460±45	-894±765	489±198
2	743±1	67±15	460±53	-1173±944	313±102
3	594±1	68±16	360±45	-1091±936	289±83

Results for LHHW 24 and 23 activation energy are similar to the bibliography while slightly higher values have been obtained for n=2 and 3. When the inhibition of water was included, much lower values have been obtained in relation to the bibliography. Also, lower value has been obtained for model LHHW-10, however this model has higher SSRR, then this value is less significant.

The difference between model 25-W and 23 is the role attributed to water. LHHW-23 assumes a strong competitive water adsorption lessening the global reaction rate, whereas LHHW 25-W supposes that a part of released water remains in the catalyst blocking or inhibiting the active centers, which has a reducing effect on the global rate constant value.[19]

6. CONCLUSIONS

All best models with thermodynamical sense suggest that the fraction of non-occupied sites is negligible, which seems reliable in liquid-phase reactions catalyzed by solids. The adsorption loss entropy estimated between nonanol and nonene is consistent. Regarding the adsorption constant, K_D/K_{H2O} seem to be consistent with molecular polarity at low temperatures, while K_D/K_N and K_N/K_{NOH} no follow a trend related to molecular polarity. All adsorption constant values are highly temperature dependent.

LHHW 24 n=1 has the apparent activation energy closer to the literature while LHHW 24 n=3 has the minimum SSRR. When the inhibition of water was included, apparent activation energy lower values have been obtained in relation to the bibliography. LHHW 25-W has very similar SSRR values with n=1,2,3. Then, no conclusive results have been obtained regarding the number of active sites involved in the rate-limiting step

Adding the water inhibition always improves the fit in terms of SSRR. This is due to the addition of parameters and the flexibility of the power expression. For the evaluated systems, it has been found that the randomness of the normalized error distribution also improves. On the other hand, adding parameters easily leads to an increased correlation between them. Finally, the model 25-W n=1 with thermodynamic sense has been obtained, which suggests that the inhibition of water takes place in this system.

7. RECOMMENDATIONS

The following recommendations are proposed:

- Perform a deeper preliminary analysis of the experimental data.
- Experimental data should include more experimental points with better distribution.
- Execute experiments with the initial mixture containing the reaction products, especially water. This would improve the inhibition factor. Then, mathematical expressions where only products are included in the denominator could be evaluated.
- Add water inhibition to more models, even those with low SSRR, because adding water inhibition greatly improves SSRR.

REFERENCES AND NOTES

1. Al-Ghussain, Loiy. Global warming: review on driving forces and mitigation. Environmental Progress & Sustainable Energy, **2019**, vol. 38, no 1, p. 13-21.
2. Rajak, Jitendra. A Preliminary Review on Impact of Climate change and our Environment with Reference to Global Warming. Int. J. Environ. Sci, **2021**, vol. 10, p. 11-14.3.
3. Bhujal, Sachin Krushna, et al. Biotechnological potential of rumen microbiota for sustainable bioconversion of lignocellulosic waste to biofuels and value-added products. Science of The Total Environment, **2022**, p. 152773.
4. Rodionova, Margarita V., et al. A comprehensive review on lignocellulosic biomass biorefinery for sustainable biofuel production. International Journal of Hydrogen Energy, **2021**.
5. Climent, Maria J.; Corma, Avelino; Iborra, Sara. Conversion of biomass platform molecules into fuel additives and liquid hydrocarbon fuels. Green Chemistry, **2014**, vol. 16, no 2, p. 516-547.
6. SHERRINGTON, David C. Preparation, structure and morphology of polymer supports. Chemical Communications, **1998**, no 21, p. 2275-2286.
7. CORAIN, Benedetto; ZECCA, M.; JERÀBEK, Karel. Catalysis and polymer networks-the role of morphology and molecular accessibility. Journal of molecular catalysis. A, Chemical, **2001**, vol. 1, no 177, p. 3-20.
8. Biffis, A., et al. On the macromolecular structure and molecular accessibility of swollen microporous resins: a combined ESR-ISEC approach. Journal of the American Chemical Society, **1995**, vol. 117, no 5, p. 1603-1606.
9. Ramírez, Eliana, et al. Role of ion-exchange resins as catalyst in the reaction-network of transformation of biomass into biofuels. Journal of Chemical Technology & Biotechnology, **2017**, vol. 92, no 11, p. 2775-2786.6.
10. Cabral, Natalia Mariano, et al. Solid acid resin Amberlyst 45 as a catalyst for the transesterification of vegetable oil. Frontiers in chemistry, **2020**, vol. 8, p. 305.
11. Du Toit, Elizabeth; Nicol, Willie. The rate inhibiting effect of water as a product on reactions catalysed by cation exchange resins: formation of mesityl oxide from acetone as case study. Applied Catalysis A: General, **2004**, vol. 277, no 1-2, p. 219-225
11. Izquierdo, José Felipe. Cinética de las reacciones químicas. Barcelona: Edicions Universitat de Barcelona, **2004**.
12. Balakos, Michael W.; Chuang, Steven SC. Dynamic and LHHW kinetic analysis of heterogeneous catalytic hydroformylation. Journal of Catalysis, **1995**, vol. 151, no 2, p. 266-278.
13. Alonso, David Martin, et al. Production of liquid hydrocarbon transportation fuels by oligomerization of biomass-derived C 9 alkenes. Green chemistry, **2010**, vol. 12, no 6, p. 992-999.
14. Soto, Rodrigo, et al. Kinetic modeling of the simultaneous etherification of ethanol with C4 and C5 olefins over Amberlyst™ 35 using model averaging. Chemical Engineering Journal, **2017**, vol. 307, p. 122-134.
15. Du Toit, Elizabeth; SCHWARZER, Renier; NICOL, Willie. Acetone condensation on a cation exchange resin catalyst: the pseudo equilibrium phenomenon. Chemical engineering science, **2004**, vol. 59, no 22-23, p. 5545-5550.
16. Yang, Bo-Lun; Maeda, Madoka; Goto, Shigeo. Kinetics of liquid phase synthesis of tert-amyl methyl ether from tert-amyl alcohol and methanol catalyzed by ion exchange resin. International journal of chemical kinetics, **1998**, vol. 30, no 2, p. 137-143

17. Perez-Maciá, María Ángeles, et al. Kinetic study of 1-butanol dehydration to di-n-butyl ether over Amberlyst 70. AIChE Journal, **2016**, vol. 62, no 1, p. 180-194.
18. Casas, Carlos, et al. Kinetics of the liquid phase dehydration of 1-octanol to di-n-octyl ether on Amberlyst 70. AIChE Journal, **2017**, vol. 63, no 9, p. 3966-3978.
19. Bringué, Roger, et al. Kinetics of 1-pentanol etherification without water removal. Industrial & engineering chemistry research, **2011**, vol. 50, no 13, p. 7911-7919.
20. Bringué, R., et al. Water effect on the kinetics of 1-pentanol dehydration to di-n-pentyl ether (DNPE) on Amberlyst 70. Topics in Catalysis, **2007**, vol. 45, no 1, p. 181-186.

ACRONYMS

- LHHW: Langmuir-Hinshelwood-Hougen-Watson.
- (GHGs): greenhouse gases.
- CO_2: carbon dioxide
- CH_4: methane
- N_2O: nitrogen oxide
- GLV : γ-valero lactone.
- NOH: 5-nonanol
- N: nonene
- $\mathrm{H_2O}$: water
- SO3H+: sulfonic acid group
- ST: styrene.
- DVB: divinylbenzene
- C5-C6: pentoses and hexoses:
- PS-DVB: polystyrene-divinylbenzene.
- SSRR: sum of squared relative errors.
- $r'_{ads,NOH}$: Net adsorption rate.
- $k_{a,NOH}$: Adsorption rate constant.
- $k_{d,NOH}$: Desorption rate constant.
- C_{NOH}: Liquid phase concentration of nonanol.
- $\hat{C}_v$: Concentration of the empty sites on the catalyst surface.
- $\hat{C}_{NOH}$: Concentration of nonanol adsorbed.
- $r'_{d,N}$: Net desorption rate of nonene.
- $r'_{d,\,H_2O}$: Net desorption rate of water.

- $k_{d,N}$ Nonene desorption rate constant.
- k_{d,H_2O} Water desorption rate constant.
- $k_{a,N}$: Nonene adsorption rate constant.
- k_{a,H_2O} : Water desorption rate constant.
- C_N Liquid phase concentration of nonene.
- $\hat{C}_N$ Concentration of nonene adsorbed
- $\hat{C}_{H_2O}$ Concentration of water adsorbed
- C_{H_2O} Liquid phase concentration of water
- ΔH_j adsorption enthalpy of compound j, $kJ/molK$
- A: pre-exponencial factor
- ΔS_j adsorption entropy of compound j, $J/mol\ K$
- r_{calc}: reaction rate computed by a rate model, mol/kg h
- $K_{a,j}$: adsorption equilibrium constant of compound j
- r_{exp} : reaction rate obtained from experiments, mol/kg h
- E_a : activation energy kJ/mol
- T: temperature K
- Tref: mean temperature K
- α : fitting parameter in Freundlich isotherm
- n: number of active centers involved in the chemical reaction
- $K\alpha$: Freundlich parameter, K
- $Kw1$: Freundlich parameter
- $Kw2$: Freundlich parameter
- ε_i : uncertainty of parameter
- b_i: fitting parameter

APPENDICES

APPENDIX 1: TABLES WITH ALL MODELS ANALYZED.

Table 15 LHHW without the effect of water

LHHW 1 (n=1,2,3)	$r' = \frac{\hat{k}\, K_{NOH} \hat{C}_0^{\,2} a_{NOH}}{\left(1 + K_{H_2O}\, a_{H_2O} + K_N\, a_N + a_{NOH} K_{NOH}\right)^n}$
LHHW 2 (n=1,2,3)	$r' = \frac{\hat{k}\, K_{NOH} \hat{C}_0^{\,2} a_{NOH}}{(1 + K_N\, a_N + K_{NOH}\, a_{NOH})^n}$
LHHW 3 (n=1,2,3)	$r' = \frac{\hat{k}\, K_{NOH} \hat{C}_0^{\,2} a_{NOH}}{\left(1 + K_{H_2O}\, a_{H_2O} + K_N\, a_N\right)^n}$
LHHW 4 (n=1,2,3)	$r' = \frac{\hat{k}\, K_{NOH} \hat{C}_0^{\,2} a_{NOH}}{\left(1 + K_{H_2O}\, a_{H_2O} + K_{NOH}\, a_{NOH}\right)^n}$
LHHW 5 (n=1,2,3)	$r' = \frac{\hat{k}\, K_{NOH} \hat{C}_0^{\,2} a_{NOH}}{(1 + K_{NOH}\, a_{NOH})^n}$
LHHW 6 (n=1,2,3)	$r' = \frac{\hat{k}\, K_{NOH} \hat{C}_0^{\,2} a_{NOH}}{(1 + K_N\, a_N)^n}$
LHHW 7 (n=1,2,3)	$r' = \frac{\hat{k}\, K_{NOH} \hat{C}_0^{\,2} a_{NOH}}{\left(1 + K_{H_2O}\, a_{H_2O}\right)^n}$
LHHW 8 (n=1,2,3)	$r' = \frac{\hat{k}\, \hat{C}_0^{\,2} a_{NOH}}{\left(a_{H_2O}\, \frac{K_{H_2O}}{K_{NOH}} + a_{NO}\, \frac{K_{NO}}{K_{NOH}} + a_{NOH}\right)^n}$
LHHW 9 (n=1,2,3)	$r' = \frac{\hat{k}\, \hat{C}_0^{\,2} a_{NOH}}{\left(\frac{K_{H_2O}}{K_{NOH}} a_{H_2O} + a_{NOH}\right)^n}$
LHHW 10 (n=1,2,3)	$r' = \frac{\hat{k}\, \hat{C}_0^{\,2} a_{NOH}}{\left(\frac{K_N}{K_{NOH}} a_N + a_{NOH}\right)^n}$

Table 16 LHHW adding dioxane (solvent)

LHHW 11 (n=1,2,3)	$r' = \frac{\hat{k}\,\hat{C_0}^{\,2} a_{NOH}}{\left(1 + \frac{K_D}{K_{NOH}} a_D + \frac{K_N}{K_{NOH}} a_N + \frac{K_{H_2O}}{K_{NOH}} a_{H_2O} + a_{NOH}\right)^n}$
LHHW 12(n=1,2,3)	$r' = \frac{\hat{k}\,K_{NOH}\hat{C_0}^{\,2} a_{NOH}}{(1 + a_D K_D + K_N a_N + K_{NOH}\, a_{NOH})^{\,n}}$
LHHW 13(n=1,2,3)	$r' = \frac{\hat{k}\,K_{NOH}\hat{C_0}^{\,2} a_{NOH}}{\left(1 + K_{H_2O}\, a_{H_2O} + K_D\, a_D + K_{NOH}\, a_{NOH}\right)^{\,n}}$
LHHW 14(n=1,2,3)	$r' = \frac{\hat{k}\,K_{NOH}\hat{C_0}^{\,2} a_{NOH}}{\left(1 + K_{H_2O}\, a_{H_2O} + K_N\, a_N + K_D\, a_D\right)^{\,n}}$
LHHW 15(n=1,2,3)	$r' = \frac{\hat{k}\,K_{NOH}\hat{C_0}^{\,2} a_{NOH}}{(1 + a_D K_D + K_{NOH}\, a_{NOH})^{\,n}}$
LHHW 16(n=1,2,3)	$r' = \frac{\hat{k}\,K_{NOH}\hat{C_0}^{\,2} a_{NOH}}{\left(1 + K_{H_2O}\, a_{H_2O} + K_D\, a_D\right)^{\,n}}$
LHHW 17(n=1,2,3)	$r' = \frac{\hat{k}\,K_{NOH}\hat{C_0}^{\,2} a_{NOH}}{(1 + K_N\, a_N + K_D\, a_D)^{\,n}}$
LHHW 18(n=1,2,3)	$r' = \frac{\hat{k}\,K_{NOH}\hat{C_0}^{\,2} a_{NOH}}{\left(\frac{K_D}{K_{NOH}} a_D + \frac{K_N}{K_{NOH}} a_N + \frac{K_{H_2O}}{K_{NOH}} a_{H_2O} + a_{NOH}\right)^n}$
LHHW 19(n=1,2,3)	$r' = \frac{\hat{k}\,\hat{C_0}^{\,2} a_{NOH}}{\left(\frac{K_D}{K_{NOH}} a_D + \frac{K_N}{K_{NOH}} a_N + a_{NOH}\right)^n}$
LHHW 20(n=1,2,3)	$r' = \frac{\hat{k}\,\hat{C_0}^{\,2} a_{NOH}}{\left(\frac{K_{H_2O}}{K_{NOH}} a_{H_2O} + \frac{K_D}{K_{NOH}} a_D + a_{NOH}\right)^n}$
LHHW 21(n=1,2,3)	$r' = \frac{\hat{k}\,\frac{K_{NOH}}{K_{H_2O}}\hat{C_0}^{\,2} a_{NOH}}{\left(a_{H_2O} + \frac{K_N}{K_{H_2O}} a_N + \frac{K_D}{K_{H_2O}} a_D\right)^n}$

LHHW 22(n=1,2,3)	$r' = \frac{\hat{k}\,\hat{C}_0{}^2 a_{NOH}}{\left(\frac{K_D}{K_{NOH}} a_D + a_{NOH}\right)^n}$
LHHW 23(n=1,2,3)	$r' = \frac{\hat{k}\,\frac{K_{NOH}}{K_{H_2O}}\hat{C}_0{}^2 a_{NOH}}{\left(a_{H_2O} + \frac{K_D}{K_{H_2O}} a_D\right)^n}$
LHHW 24(n=1,2,3)	$r' = \frac{\hat{k}\,\frac{K_{NOH}}{K_N}\hat{C}_0{}^2 a_{NOH}}{\left(a_N + \frac{K_D}{K_N}\, a_D\right)^n}$
LHHW 25(n=1,2,3)	$r' = \frac{\hat{k}\,K_{NOH}\hat{C}_0{}^2 a_{NOH}}{(K_D a_D)^n}$

Table 17 Group 3 LHHW with inhibition effect of water

LHHW 6-W (n=1,2,3)	$r' = \hat{k}\,K_{NOH}\hat{C}_0{}^2 a_{NOH}\left(\frac{1 - K_W\, a_{H_2O}{}^{\frac{1}{\alpha}}}{1 + K_N\, a_N}\right)^n$
LHHW 10-W (n=1)	$r' = \hat{k}\,\hat{C}_0{}^2 a_{NOH}\left(\frac{1 - K_W\, a_{H_2O}{}^{\frac{1}{\alpha}}}{\frac{K_N}{K_{NOH}} a_N + a_{NOH}}\right)^n$
LHHW 24-W (n=1,2,3)	$r' = \hat{k}\,\frac{K_{NOH}}{K_N}\hat{C}_0{}^2 a_{NOH}\left(\frac{1 - K_W\, a_{H_2O}{}^{\frac{1}{\alpha}}}{a_N + \frac{K_D}{K_N}\, a_D}\right)^n$
LHHW 25-W (n=1,2,3)	$r' = \hat{k}\,\frac{K_{NOH}}{K_D}\hat{C}_0{}^2 a_{NOH}\left(\frac{1 - K_W\, a_{H_2O}{}^{\frac{1}{\alpha}}}{a_D}\right)^n$

APPENDIX 2: MODELS MODIFIED BY THE ADDITION OF WATER INHIBITION FIGURES.

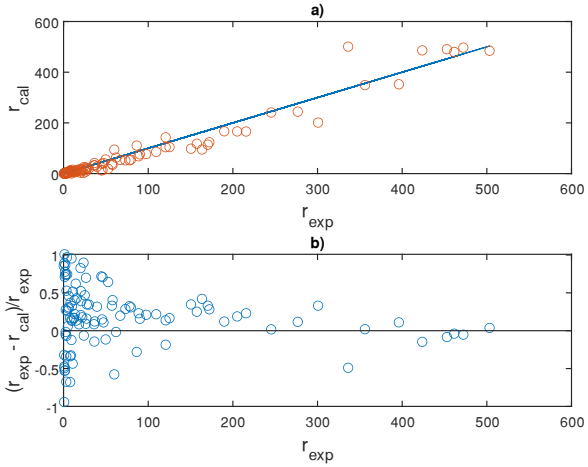

Figure 29 Calculated reaction rates versus experimental reaction rates and residual LHHW 6-W n=1

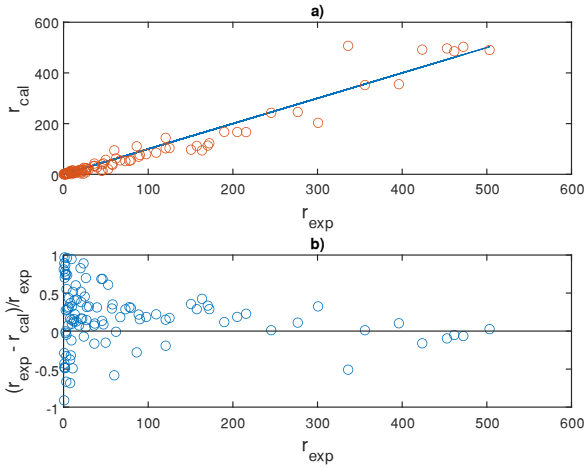

Figure 30 Calculated reaction rates versus experimental reaction rates and residual LHHW 6-W n=2

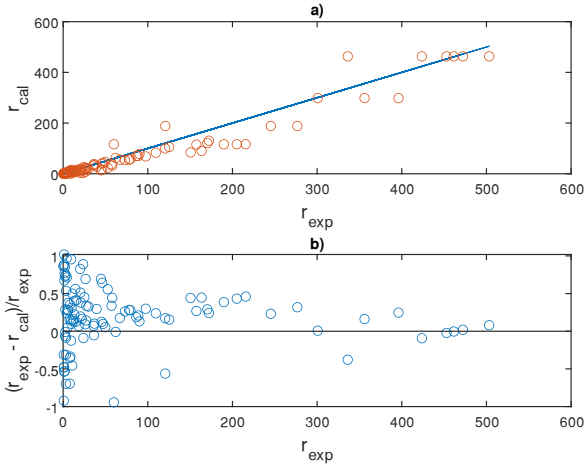

Figure 31 Calculated reaction rates versus experimental reaction rates and residual LHHW 6-W n=3

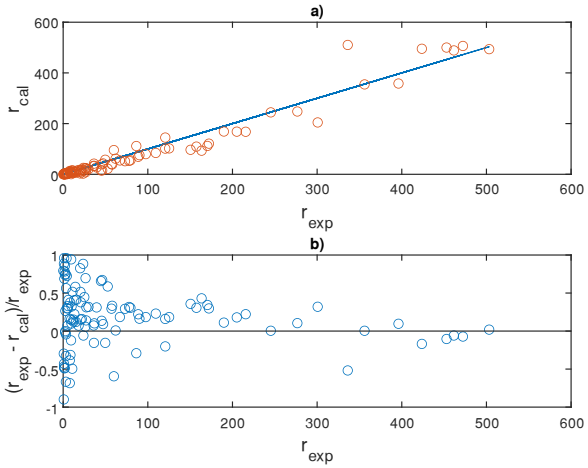

Figure 32 Calculated reaction rates versus experimental reaction rates and residual LHHW 10-W n=1

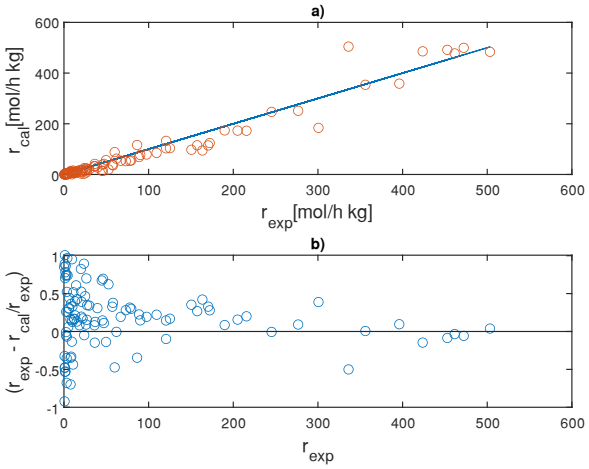

Figure 33 Calculated reaction rates versus experimental reaction rates and residual LHHW 24-W n=1

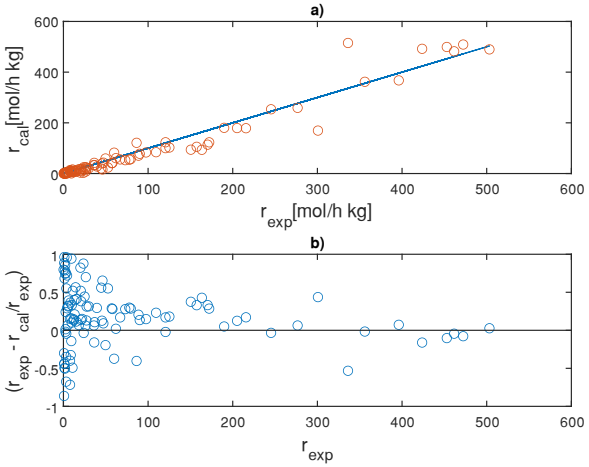

Figure 34 Calculated reaction rates versus experimental reaction rates and residual LHHW 24-W n=2

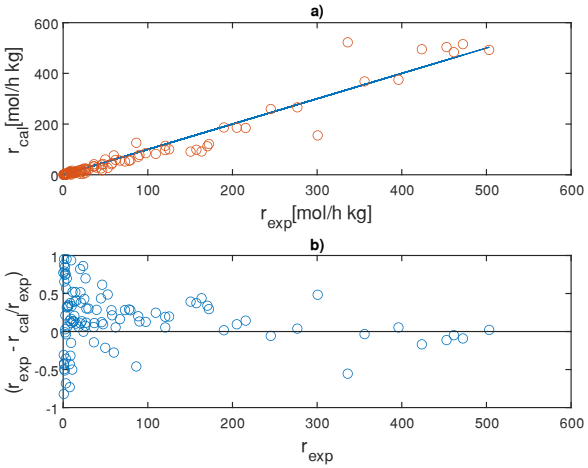

Figure 35 Calculated reaction rates versus experimental reaction rates and residual LHHW 24-W n=3